

ESIEE
AMIENS

CHALMERS



Thermal Modelling of a Transformer based on PT-1000 Sensor

Rapport de STAGE I4 GEDD 2013 - 2014

ELEVE

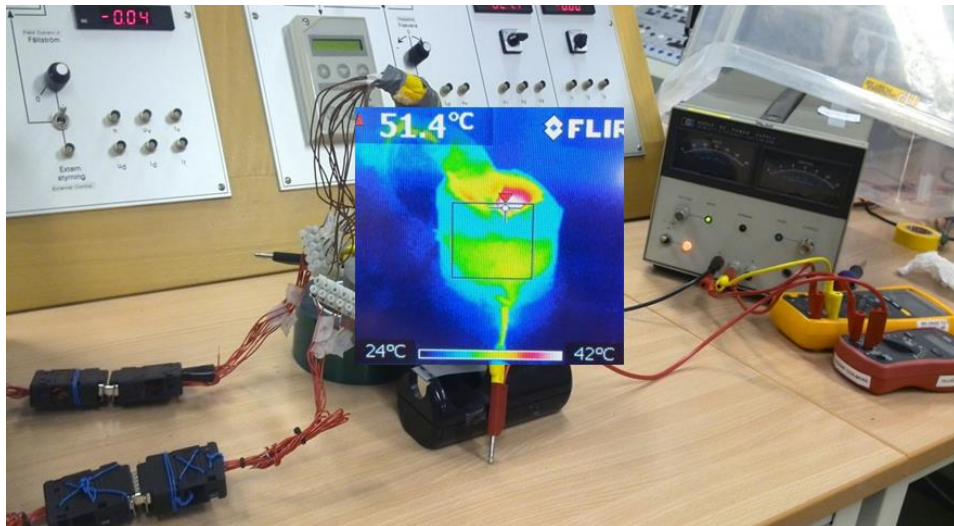
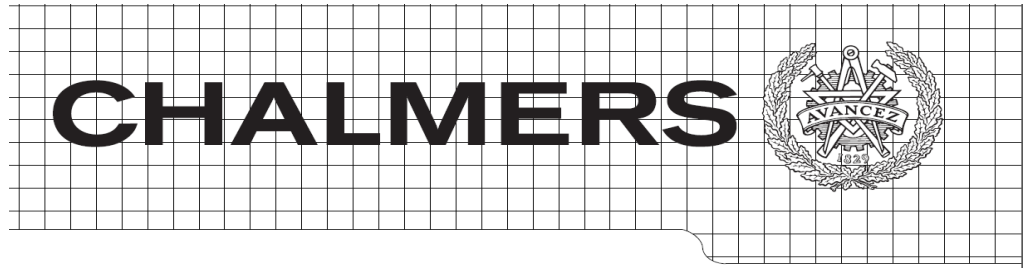
Junxing HUANG

TUTEUR UNIVERSITE

Torbjörn Thiringer

TUTEUR ESIEE

Olivier MALOBERTI



Thermal Modelling of a Transformer based on PT-1000 Sensor

Fourth year project (I4 STAGE en Chalmers)

Junxing HUANG

Department of Energy and Environment
Division of Electric Power Engineering
CHALMERS UNIVERSITY OF TECHNOLOGY
SE-412 96 Gothenburg, Sweden 2014

Thermal Modelling of a Transformer based on PT-1000 Sensor

Department of Energy and Environment
Division of Electric Power Engineering
CHALMERS UNIVERSITY OF TECHNOLOGY
SE-412 96 Gothenburg, Sweden 2014

Thermal Modelling of a Transformer based on PT-1000 Sensor

Junxing HUANG

© Junxing HUANG 2014

Department of Energy and Environment

Division of Electric Power Engineering

CHALMERS UNIVERSITY OF TECHNOLOGY

SE-412 96 Gothenburg,

Sweden 2014

Telephone +46 (0)31-772 1000

Cover:

A thermal image from a transformer

Chalmers Bibliotek Reproservice

Gothenburg, Sweden 2014

Abstract

We can calculate the Joule losses according to the principle $P=RI^2$ in an electrical machine and transformer. However, the total loss is harder to determine because of the complicated electromagnetic factor, such as excess iron losses or the way the heat is transferred for example, it will be a difficulty to evaluate the temperature rise which is likely to exceed the limit of temperature during its use. Thus a temperature prediction based on an accurate measurement system is needed.

This work aims at the thermal modelling of a multilayer wire-wound transformer and its verification by using the temperature sensors of the type PT-1000. In order to achieve this goal, firstly, a brief introduction about the data acquisition system including PCB and LabVIEW was made. Then two main tests were carried out. For the first one, a transformer without any interlayer thermal insulation was constructed. This test focused on the measurement of thermal resistance by using an external heating source to create a one-dimension heat flow. On the basis of these results, the temperature of each layer could be predicted when the windings were conducted with DC power in a real application. This prediction model applied to any DC current but was only suitable for the transformer made in test 1. For the second test, the theoretical thermal resistances were firstly calculated based on the material which was used to manufacture the transformer. Then the comparison between the theoretical and measured values was performed. The most important usage of this model lied on the applicability to all the similar transformers.

When all the thermal resistances in each part were decided, a whole thermal network was presented.

Key words: Thermal Modelling, PT-1000, Transformer, PLECS, LabVIEW Software.

Acknowledgement

This project has been fund by Conseil R égional de Picardie and ERASMUS. I express my greatest gratitude for their financial supports.

I would like to give my sincere and respectful thanks to my examiner Torbjörn Thiringer in Chalmers University of Technology and my examiner Olivier MALOBERTI in ESIEE-Amiens. They could always give me the constructive advice and helpful guidance through my entire project. I really appreciate their patience, immense knowledge and enthusiasm to the work. Thank you!

My thanks also go to my supervisors Mohammadamin Bahmani and Tarik Abdulahovic, who gave me many insightful comments and the best suggestions.

Besides, my acknowledgements go to Robert Karlsson and Magnus Ellsen for providing me the necessary materials and equipment as well as an advanced experiment platform.

In addition, I am grateful to the coordinators within ERASMUS, especially Anne LEMAIRE and Ing-Britt Carlsson, for their administrative supports.

Last but not least, I would like to thank my families, my beloved fiancé for their love and giving me the chance to go abroad.

Junxing HUANG

Gothenburg, Sweden 2014

Contents

Abstract	i
Acknowledgement.....	iii
1. Introduction	1
1.1 Problem background	1
1.2 Delimitations	1
1.3 Purpose of the work.....	2
2. Technical background	3
2.1 General theory of transformer	3
2.2 Energy losses in a real transformer	4
2.3 Temperature coefficient of resistance	6
2.4 Thermal theory	6
3. Temperature measurement system	11
3.1 Introduction of the temperature measurement system	11
3.2 The function blocks of the temperature measurement system	12
3.2.1 RTD PT-1000 Sensor	12
3.2.2 PT-1000 sensor in the Wheatstone bridge.....	13
3.2.3 Amplifier INA122	15
3.2.4 Low-pass filter circuit	16
3.2.5 Introduction of the Printed Circuit Board	18
3.3 Data handling system	21
3.3.1 LabVIEW	21
3.3.2 Calibration.....	23
3.3.3 Matlab.....	25
4. Manufacture procedure.....	27
4.1 Materials for the construction of transformer	27
4.2 Characteristic parameters of the materials	28
4.3 Transformer construction	29
4.3.1 Construction step.....	31
5. Experiment set-up and test analysis	35
5.1 Experiment set-up	35
5.1.1 Thermal model	35
5.1.2 Determination of the excitation resource P	37
5.2 Test 1- No interlayer thermal insulation	37
5.2.1 External heating source	37
5.2.2 Internal heating source	42
5.2.3 Simulation in PLECS	46
5.2.4 Conclusion for test 1	51
5.3 Test 2- With interlayer thermal insulation	51
5.3.1 Heating source.....	51
5.3.2 Coil former test.....	52
5.3.3 Core test.....	55
5.3.4 Windings test.....	59
5.3.5 The whole thermal network.....	65
6. Conclusion and future work	67
6.1 Conclusion.....	67
6.2 Future work	67
References	69

Appendix A 71
Appendix B 79
Appendix C 91

Chapter 1

1. Introduction

1.1 Problem background

Nowadays, many studies about thermal modelling of large transformers based on FEM (Finite Element Method) have been made. However, the studies on building a thermal model of a small inductor or a small transformer are less frequent. In most cases, they are considered to be an ideal component by neglecting electrical or magnetic losses which occur in the materials used to construct the device.

With the rapid development in industries regarding lowering power dissipation, the miniaturization of electronic products is becoming an inevitable trend. In other words, the problem of heat dissipation in a compact system will turn out to be a bottleneck to this development.

An inductor or a small transformer is one essential part for most electronic systems. For a compact design, the heat dissipation cannot be neglected. It is necessary to know the electrical and thermal properties in a certain system for the purpose of calculating a safe current range. Under this condition, we do not need to worry about the risk of a system crash because of an over load, on the other hand, we do not want to waste copper material caused by an over dimensioning. So these aspects must be considered in designing some functional block such as a filter circuit or a DC chopper circuit.

To sum up, the temperature has become one of the most vital factors to predict the behavior of a system. Accordingly, there is a need for good thermal models and also measurement verification of the models.

1.2 Delimitations

This internship aims at performing thermal modelling in order to predict the temperature behavior of a small inductor or small transformer. It is not suitable for larger transformers such as oil transformers, resinated dry type transformer or planar transformers. Moreover, this project has to be finished within a timeframe of 14 weeks which is far away from the time needed to take everything into consideration. So for the component of interface between data collecting and handling it was possible to use an existing PCB.

1.3 Purpose of the work

The first purpose of this thesis work is to build a transformer entity in which we can collect the measurement data based on PT-1000 temperature sensors and LabVIEW.

Secondly, according to the measured data and the analysis of the results we can deduce a practical thermal modelling which will compare with the thermal model based on theories.

Moreover, by setting up a thermal modelling we can know precisely the energy loss during the energy transformation. Thus we can offer some necessary parameters to design an electronic circuit taking the heat flow into consideration.

In this training course, the winding will be mainly connected to DC voltage to measure its Joule losses. Compare to the using of AC voltage, the biggest difference lies on the omission of total magnetic losses into the iron core.

Chapter 2

2. Technical background

This chapter concerns the principle of a transformer and the losses generated by a transformer. At the same time, it presents some thermal theories.

2.1 General theory of transformer

A transformer is a static electrical device which transfers energy between two circuits through electromagnetic induction. It may be used as a safe and efficient voltage converter to change the AC voltage at its input to a higher or lower voltage at its output. In an electrical system, the transformer plays a very important role in the power energy economical transportation and the flexible distribution as well as the safe energy use.

Commonly, a transformer consists of two windings of wire (single-phase transformer) or more windings of wire that are wrapped around a common core to provide tight electromagnetic coupling between the windings. The primary winding must be connected to an alternating voltage source (V_p) in order to generate a flow of alternating flux (ϕ) whose magnitude depends on the voltage and number of turns of the primary winding (N_p). The alternating flux links the secondary winding and induces a voltage (V_s) in it with a value that depends on the number of turns of the secondary winding (N_s). This model is shown in Fig. 2.1[1].

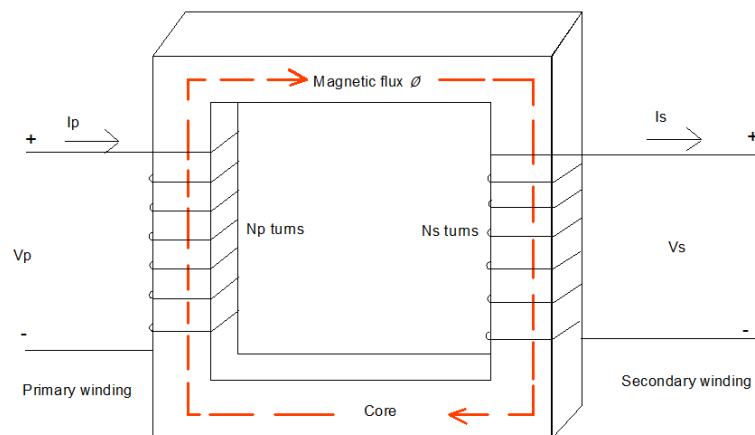


Fig. 2.1: Transformer Ideal Model

We assume that the Electromotive Force (EMF) produced in the primary winding is ξ_1 and the EMF in the second winding is ξ_2 . According to the Faraday's law, we can deduce (neglecting the winding resistance):

In the primary winding,

$$V_p = \xi_1 = N_p \left(\frac{d\phi}{dt} \right) \quad (2.1)$$

In the secondary winding,

$$V_s = \xi_2 = N_s \left(\frac{d\phi}{dt} \right) \quad (2.2)$$

As a result we can represent

$$\frac{V_s}{V_p} = \frac{N_s}{N_p} = n \quad (2.3)$$

where n is the ratio of transformation for voltage.

For an ideal transformer, the instantaneous power transferred in both sides is equal. Thus we can get,

$$V_p I_p = V_s I_s \quad (2.4)$$

Combining (2.3) and (2.4), we have,

$$\frac{I_s}{I_p} = \frac{N_p}{N_s} = \frac{1}{n} \quad (2.5)$$

Hence the current ratio is the inverse of the voltage ratio.

2.2 Energy losses in a real transformer

The ideal transformer model above does not include any energy loss. Nevertheless for a real transformer, it is just 95% to 99.5% efficient because of several losses mechanisms which are presented below:

- Winding joule losses

These losses are also known as copper losses and they are caused by the internal resistance in both sides of the real transformer. They can be conducted by the formula,

$$P=RI^2 \tag{2.6}$$

Thus the Joule losses depend upon the load of a transformer. When frequency increases, skin effect and proximity effect also cause an additional winding resistance and, hence, an increase to losses.

- Core losses

These losses include Hysteresis Losses and Eddy Current Losses. For the former, basing on the Steinmetz's formula, the heat energy is given by,

$$P_h \approx \eta f B_{\max}^{1.6} \tag{2.7}$$

where f is the frequency, η is the hysteresis coefficient and B_{\max} is the peak flux density. When the transformer is subjected to an alternating current (AC), an induced current (eddy current) will be created in the core made of ferromagnetic materials. These eddy current losses in a transformer are denoted as,

$$P_e \approx K_e f^2 K_f^2 B_{\max}^2 \tag{2.8}$$

where K_e is the eddy current coefficient and K_f is the coefficient of the form.

From (2.7) and (2.8), we can notice that the core losses depend on magnetic properties of the materials other than the load current, so these losses can be considered to be constant once the transformer is made.

In this thesis work, the second winding will not be made. The equivalent circuit can be presented in Fig. 2.2,

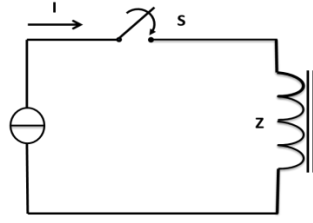


Fig. 2.2: Equivalent circuit for a transformer conducted with DC

2.3 Temperature coefficient of resistance

During the thermal modelling, we cannot neglect the resistance variation caused by the temperature. For most metals, they have a positive temperature coefficient (PTC) which means that the resistance increases with the temperature and the change in resistance is expected to be proportional to the temperature change,

$$R_T = R_0(1 + \Delta T\alpha) \quad (2.9)$$

where: $\Delta T = T - T_0$

T: the temperature at which the resistance is measured

T_0 : the reference temperature

α : the temperature coefficient

R_0 : the resistance measured at temperature T_0

R_T : the resistance measured at temperature T

For copper and pure platinum at $T_0=20^\circ\text{C}$, α will be 0.393%. [2]

2.4 Thermal theory

A transformer mainly consists of coils and iron core. So its heat dissipations mainly include two parts: losses of coils and losses of iron core. For the former, most of it are dissipated directly into the air and only a small percentage of it will get through the iron core and then is dissipated into the air. For the latter, the great part of it will also be dissipated directly into the air and a small proportion is dissipated through the coils.

Generally, there are three thermal transports mechanisms as following,

- Conduction: 'is the transfer of energy through matter from particle to particle' [3] that is to say the conduction can take place in all sorts of materials such as liquids, solids, gases or plasmas. The premise is that the materials must have contact directly or indirectly. In

the transformer, the heat will be conducted between the coils and the iron core. For one-dimensional form, Fourier's law of heat conduction can be used,

$$q_x = -kA \frac{\partial T}{\partial x} \quad (2.10)$$

where q_x is the heat-transfer rate, k is the thermal conductivity, A is the area, $\frac{\partial T}{\partial x}$ is the temperature gradient in the direction of the heat flow, the minus sign means the direction of the heat flow.

- Convection: is a more complicated method of heat transport than conduction. 'Convection is the transfer of heat by the actual movement of the warmed matter.' [3] It can take place in gas or liquid by movement of currents. So convection depends upon the temperature difference and the heat area. It can be presented as

$$Q_{convection} = \Delta T h A \quad (2.11)$$

where, $Q_{convection}$: Heat transferred per unit time (W)

ΔT : Temperature difference between the surface and the bulk fluid (°C)

h : Convective heat transfer coefficient of the process (W .m⁻². °C⁻¹)

A : Heat transfer area of the surface (m²) [4]

- Radiation: is a process in which the electromagnetic waves (EMR) travel. As we know that the EMR can propagate even in a vacuum, it transfers the energy regardless of nothing. So it's the same for radiation.

For a small size transformer, the conduction and the convection are the two predominant modes during the heat dissipation [5]. Thus for simplicity reasons, we can replace the radiation by augmenting the coefficient h of the convection.

In this work, while we conduct with DC, the iron core losses will in this case be zero. In order to avoid some misunderstandings or misconception, it is essential to know the difference as well as the similarity between the electrical and thermal domains. See Table 2.1.

Table 2.1: Definition of physical magnitudes

Electrical			Thermal		
Description	symbol	units		symbol	units
“Ohm’s Law”	$R = V / I$		“Ohm’s Law”	$R_{th} = \Delta T / P_{th}$	
Electrical Potential	V	Volts	Temperature difference	T	°C or K
Electrical Resistance	R	Ohms	Thermal Resistance	R_{th}	°C/W or K/W
Electrical Capacitance	C	F or Coulombs/V	Thermal Capacitance	C_{th}	J / °C
Electrical current	I	A or Coulombs/s	Heat flow	P_{th}	W or J / s

From the table above, we can deduce easily the energy loss led by the coils,

$$P_{ele} = RI^2 \quad (2.12)$$

These electrical losses P_{ele} turn into the heat effect and equal to P_{th} , so we have,

$$P_{th} = \frac{\Delta T}{R_{th}} \quad (2.13)$$

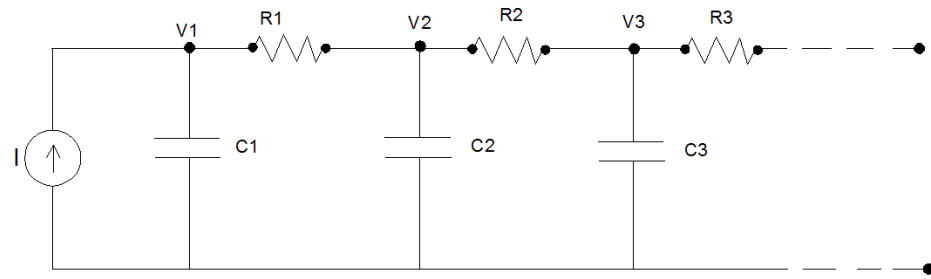
where ΔT is the difference in temperature .

We also can say

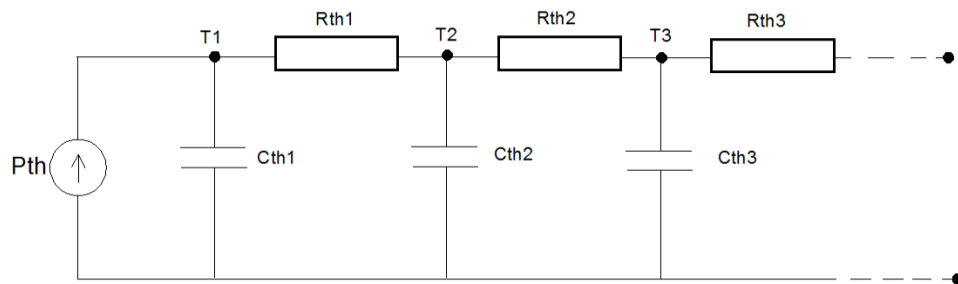
$$P_{th} = \frac{\Delta Q}{\Delta t} \quad (2.14)$$

where ΔQ is heat flow difference , Δt is time difference.

So we get two equivalent circuits illustrated in Fig. 2.3 for the general cases,



(a)



(b)

Fig. 2.3: Equivalent circuit for electrical circuit (a) and thermal circuit (b)

Chapter 3

3. Temperature measurement system

In this chapter, several parts will be presented:

Firstly, an introduction of the temperature measurement system will be given and the reason why this system is chosen will be given. Secondly, some work about the calibration during the experiment will be made. Finally the procedure of how to build a transformer will be explained.

3.1 Introduction of the temperature measurement system

To measure the temperature, we presently have many choices, for example, Mercury-in-glass Thermometer, Alcohol Thermometer, Kerosene Thermometer etc. All of them are designed according to the principle of heat-expansion and cold-contraction. They have advantages of low-cost and simplicity but also have limits such as narrow measurable range and low-accuracy. Besides, we can use the other type of thermometers, such as resistance thermometers also called Resistance Temperature Detectors (RTDs) which are made from the pure materials. Even more you can choose a Thermocouple consisting of two dissimilar conductors that connect to each other at one or more spots [6].

Generally, in order to decide which measurement method is the preferable one, the factors as follow should be taken into account,

Firstly, the environment conditions in which the measurement element will be used: the temperature range, the pressure, the weather condition etc. Then the sensed medium: the element will be attached to a surface or immersed in solid, liquid or gas; finally the precise requirement in sensing accuracy, repeatability, stability and response time and so on [7].

In this thesis work, the temperature elements will be wrapped into the transformer windings which have five layers, so they must be contact-temperature sensors. Moreover, according to the Insulation Class, the highest temperature of an operating transformer can reach 180°C (H class), [8] which means we need a sensor that can measure the temperature varying from the ambient temperature (about 20°C) to less than 200 °C. Furthermore, we have a high demand in accuracy and expect to change the measured temperature signals into electrical signals. Thus we can choose thermocouple or RTD. For the case where temperature exceeds 500°C, the thermocouple is the best choice. But for those situations where temperature is below

500°C, the RTD will be more preferable due to its higher accuracy and lower drift characteristic. So I decided to use a RTD based measurement system [9].

3.2 The function blocks of the temperature measurement system

3.2.1 RTD PT-1000 Sensor

As it has been mentioned above, the RTD element is made from a pure material having a PTC which means that its resistance increases with temperature. Theoretically, all the metal can be used to make a RTD, but platinum, nickel or copper are used frequently. More precisely, the platinum is the best and the most popular metal for RTD due to its stable and linear resistance-temperature relationship over the largest temperature range (-272.5 °C to 961.78 °C) as well as its chemical inertness.

From (2.9), we can derive the temperature coefficient

$$\alpha = \frac{R_T - R_0}{R_0 \Delta T} \quad (3.1)$$

where α is the significant characteristic of a metal used as a resistive element in RTD. It can be defined by the linear approximation between the resistance and the temperature from 0°C to 100 °C. So (3.1) can be presented

$$\alpha = \frac{R_{100} - R_0}{100 R_0} \quad (3.2)$$

where R_{100} is the resistance of the sensor at 100°C

R_0 is the resistance of the sensor at 0 °C

In order to determine the resistance-temperature relationship, an important equation which is known as Callendar–Van Dusen equation is commonly used [10],

$$R_t = R_0 [1 + At + Bt^2 + C(1 - 100)t^3] \quad (3.3)$$

where R_0 : RTD resistance at 0 °C

R_t : RTD resistance at t °C

A, B, C : Callendar-Van Dusen coefficients

t : temperature (°C)

Among the three constants above, C is used for temperature below 0°C only. So in the measurement of the transformer, $C=0$. We can turn (3.3) into

$$t = \frac{-R_0A + \sqrt{(R_0A)^2 - 4R_0B(R_0 - R_t)}}{2R_0B} \quad (3.4)$$

As long as we know the value of Callendar-Van Dusen coefficients, R_0 and R_t , we can calculate the temperature.

The typical value of A , B and C in the equation (3.3) for Platinum RTD can be defined by one of the three standards shown in Table 3.1 [11],

Table 3.1: Callendar-Van Dusen Coefficients

Standard Temperature	Coefficient α (/°C)	A (/°C)	B (/°C ²)	C (/°C ⁴)
DIN 43760	0.00385	3.9080×10^{-3}	-5.8019×10^{-7}	-4.2735×10^{-12}
American	0.003911	3.9692×10^{-3}	-5.8495×10^{-7}	-4.2325×10^{-12}
ITS-90	0.003926	3.9848×10^{-3}	-5.870×10^{-7}	-4.0000×10^{-12}

In this work, the parameters of PT-1000 sensor will be taken from the standard DIN 43760 and its nominal resistance at 0 °C is 1000Ω. Table 3.2 shows the main parameters of the PT-1000 sensor used in this work.

Table 3.2: The main parameters of the PT-1000 sensor

Type	Inaccuracy	Dimension L*W*H	Temperature coefficient	Measuring range
FK422 PT-1000 B	Class B ±0.4°C @ 20°C ±0.8°C@100°C	4.0 x 2.2 x 0.9 mm	$3.850 \times 10^{-3} (^{\circ}\text{C}^{-1})$	-70...+500 °C

3.2.2 PT-1000 sensor in the Wheatstone bridge

To measure the resistance of PT-1000 sensor, one easy way is that we can pass a known current and then measure the voltage, according to Ohms law the resistance can be computed.

Besides, the Wheatstone bridge can also be used to fulfil this purpose. This circuit shown as Fig. 3.1 consists of 4 resistors in which 3 are fixed and the other one (R_t) is the variable one.

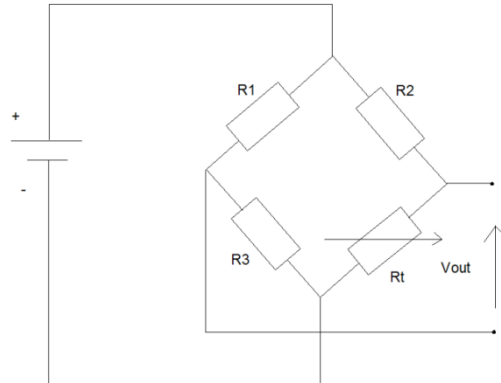


Fig. 3.1: The equivalent circuit of Wheatstone bridge

where $R_1=R_2=R_3=R$. By conducting with a constant input V_{in} we can get the relationship between the output V_{out} and R_t .

$$V_{out} = \left(\frac{R_t}{R_t+R_2} - \frac{R_3}{R_3+R_1} \right) V_{in} \quad (3.5)$$

$$V_{out} = \left(\frac{R_t}{R_t+R} - \frac{1}{2} \right) V_{in} \quad (3.6)$$

With the variation of the resistance of R_t , the V_{out} will change. So a curve showing their relationship can be presented in Fig. 3.2.

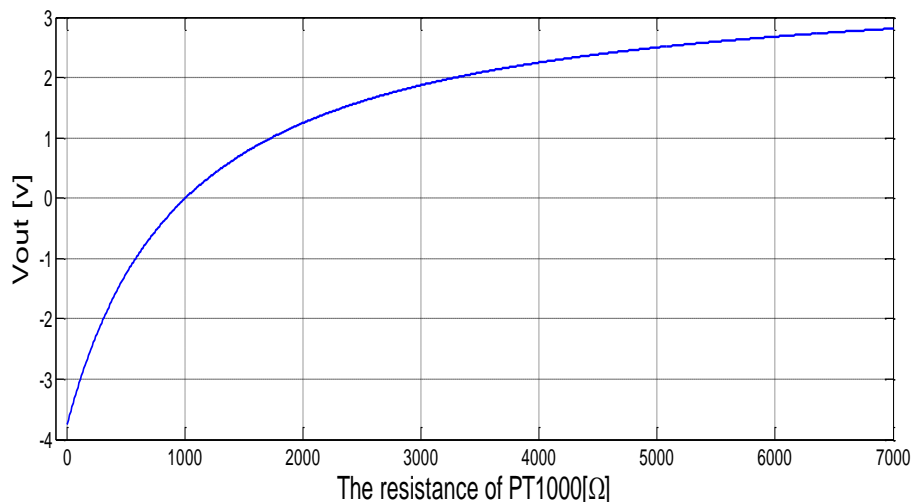


Fig. 3.2: The relationship between V_{out} and R_t

3.2.3 Amplifier INA122

As the nominal resistance of PT-1000 sensor at 0 °C has been chosen to 1000Ω, the value of R_1 , R_2 and R_3 will be set to 1000Ω so that the output V_{out} equals zero at 0 °C. With the augmentation in R_t , the Wheatstone bridge becomes unbalanced and V_{out} will change. Generally, the output V_{out} is so small that it can lead to a slight error during the calculation, thus we need an amplifier circuit.

Here an amplifier INA122 has been chosen due to its characteristic in accurate, low noise differential signal acquisition [12].

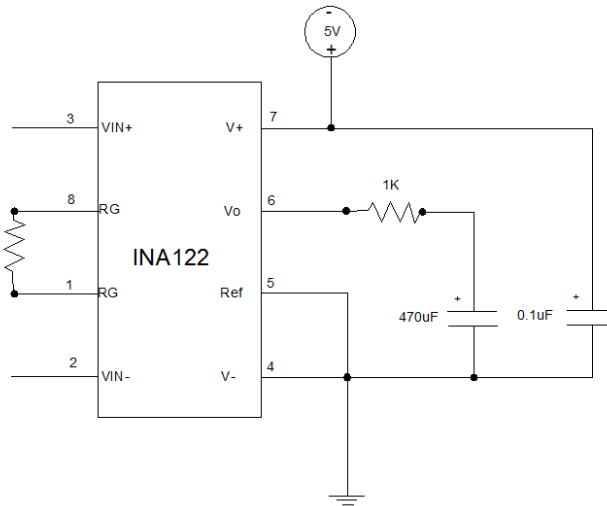


Fig. 3.3: INA122 amplifier circuit

This is a differential amplifier circuit, the voltage signal V_{out} coming from the Wheatstone bridge will be connected to V_{IN+} and V_{IN-} . The final output V_0 is determined by the equation as follows,

$$V_o = (V_{IN+} - V_{IN-})G \quad (3.7)$$

where G is the gain of INA122.

Through the amplifier circuit, the input voltage signal will be amplified by G times. Here G is decided by the value of the external resistor R_G according to the equation below,

$$G = 5 + \frac{200k}{R_G} \quad (3.8)$$

where the $200k\Omega$ term comes from the internal metal film resistors in INA122. By connecting with different R_G , we can vary the gain level from 5 to 10000 as shown in Table 3.3.

Table 3.3: The gain of the amplifier for different R_G values

Desired gain (V/V)	R_G (Ω)
5	NC
10	40k
20	13.33k
50	4444
200	1026
500	404
1000	201
2000	100.3
5000	40
10000	20

where NC means no connection.

In this experiment, G is selected to be 5. So R_G is not connected. Equation (3.7) can be transferred to

$$V_o = 5(V_{IN+} - V_{IN-}) \quad (3.9)$$

The INA122 has a wide power supply range which can vary from 2.2V to 36V DC. Here it will be powered by 5V DC. In order to stabilize the source, an IC of stabilizer 78L05 is used as well as a capacitor of 0.1uF is connected between the pin V+ and the ground [12].

3.2.4 Low-pass filter circuit

As shown above in Fig. 3.3, a simply RC low-pass filter circuit is presented for the purpose of eliminating the possible interference originating the output V_o . This part is shown in Fig. 3.4,

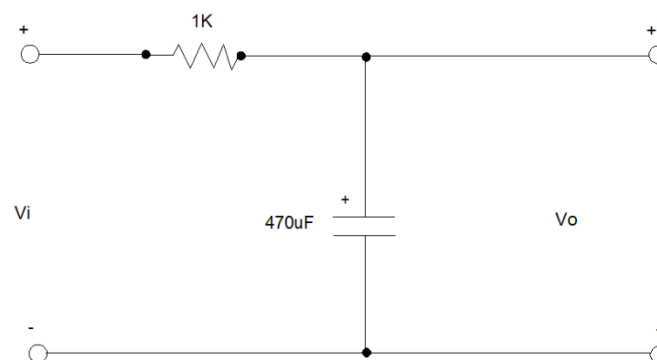


Fig. 3.4: Low-pass filter circuit

By applying the Laplace transform, we can get the transfer function of the low-pass filter as follows [13].

$$H(s) = \frac{V_o(s)}{V_i(s)} = \frac{\frac{1}{sC}}{R + \frac{1}{sC}} = \frac{1}{1+sRC} \quad (3.10)$$

where $H(s)$ is the coefficient of the transfer function.

For the practical frequency

$$s = j\omega = j2\pi f \quad (3.11)$$

The cut-off frequency can be presented by

$$f_c = \frac{1}{2\pi RC} \quad (3.12)$$

when $R=1k$, $C=470\mu F$, then $f_c = 0.338Hz$

Combining (3.10), (3.11) and (3.12), we can derive

$$H(s) = \frac{V_o(s)}{V_i(s)} = \frac{1}{1+j(\frac{f}{f_c})} \quad (3.13)$$

So the amplitude of $H(s)$ is

$$|H(s)| = \frac{1}{\sqrt{1+(\frac{f}{f_c})^2}} \quad (3.14)$$

The angle of $H(s)$ is

$$\varphi(H) = -\arctan(\frac{f}{f_c}) \quad (3.15)$$

From (3.12), we can easily derive how a low-pass filter circuit works,

- If $f \gg f_c$ which means $(\frac{f}{f_c})^2$ tends to be ∞ , so $|H(s)| = 0$
- If $f \ll f_c$ which includes $f = 0$ in the DC input, $|H(s)|$ tends to be 1

- If $f = f_c$ which means the magnitude decreases by 3db, $|H(s)| = 0.707$, $\varphi(H) = -45^\circ$. Refer to Fig. 3.5.

To sum up, the low-pass filter circuit rejects a signal with high frequency. Table 3.4 shows the main output noise frequencies in INA122 [12].

Table 3.4: The main output noise frequencies in INA122

Voltage Noise	Typical Values	Unit
$f = 1\text{kHz}$	60	$\text{nV}/\sqrt{\text{Hz}}$
$f = 100\text{Hz}$	100	$\text{nV}/\sqrt{\text{Hz}}$
$f = 10\text{Hz}$	110	$\text{nV}/\sqrt{\text{Hz}}$
$f_B = 0.1\text{Hz to } 10\text{Hz}$	2	$\mu\text{Vp-p}$

From Table 3.4, we can know that the principal noises vary from 10Hz to 1 kHz. Thus most of the noises can be filtered because of $f_c = 0.338 \text{ Hz}$.

Fig. 3.5 shows the Bode diagram of the amplitude-frequency response and the phase-frequency response obtained in Matlab.

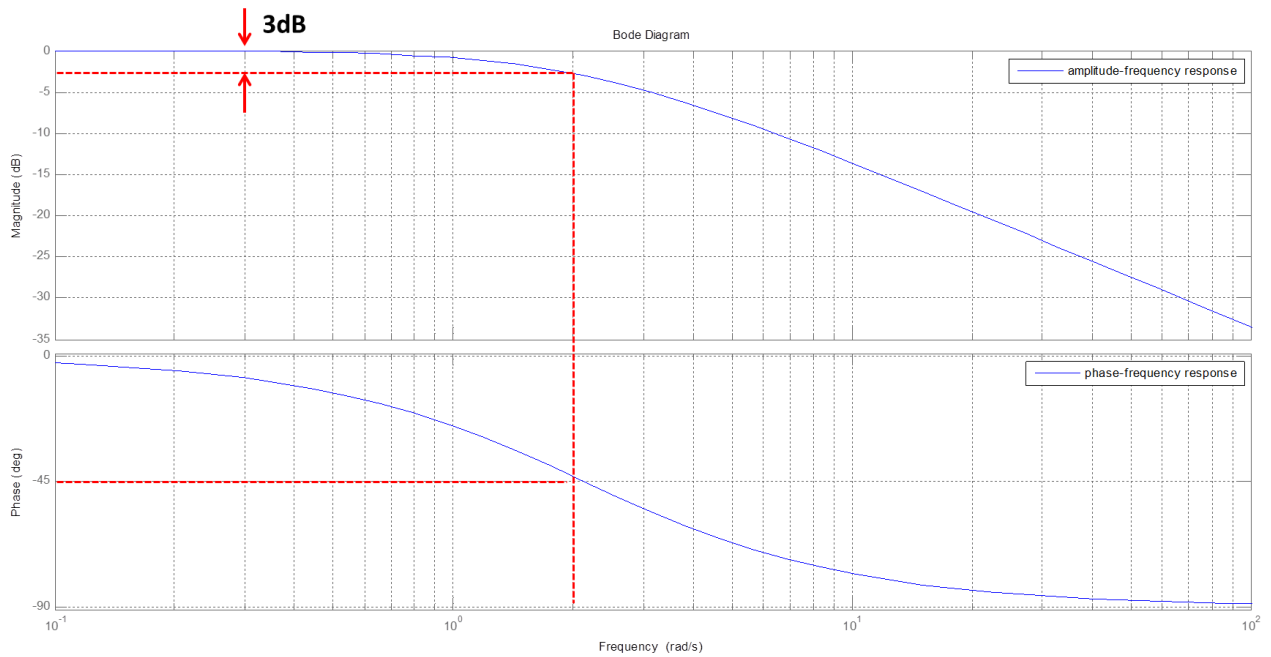


Fig. 3.5: Amplitude-frequency response and phase-frequency response

3.2.5 Introduction of the Printed Circuit Board

In order to impact and stabilize the temperature measurement system, the Wheatstone bridge, the amplifier circuit, the low-pass filter circuit and the other necessary accessories have been integrated into a Printed Circuit Board (PCB). PCB is an isolated board where all the electrical components are connected electrically by using copper traces in each layer. For

designing the PCB we can use the software PROTEUS to convert a schematic circuit to a PCB layout. PROTUES is an Electronic Design Automation (EDA) tool provided by the British company Labcenter Electronics. It is also a platform which combines the circuit simulation, the PCB design and the visual mode simulation [14].

In this work, because of the limit of time, I will use directly two existing PCBs to implement the measurement. Each PCB contains 5 input ports which mean it has 5 Wheatstone bridges inside. For obtaining a stable 5V voltage source, a three terminal voltage regulator (78L05) is also used. The PCB has 2 layers in which the top one is used for the positive supply voltage and the bottom one for the ground.

Fig. 3.6 shows the schematic circuit of the PCB,

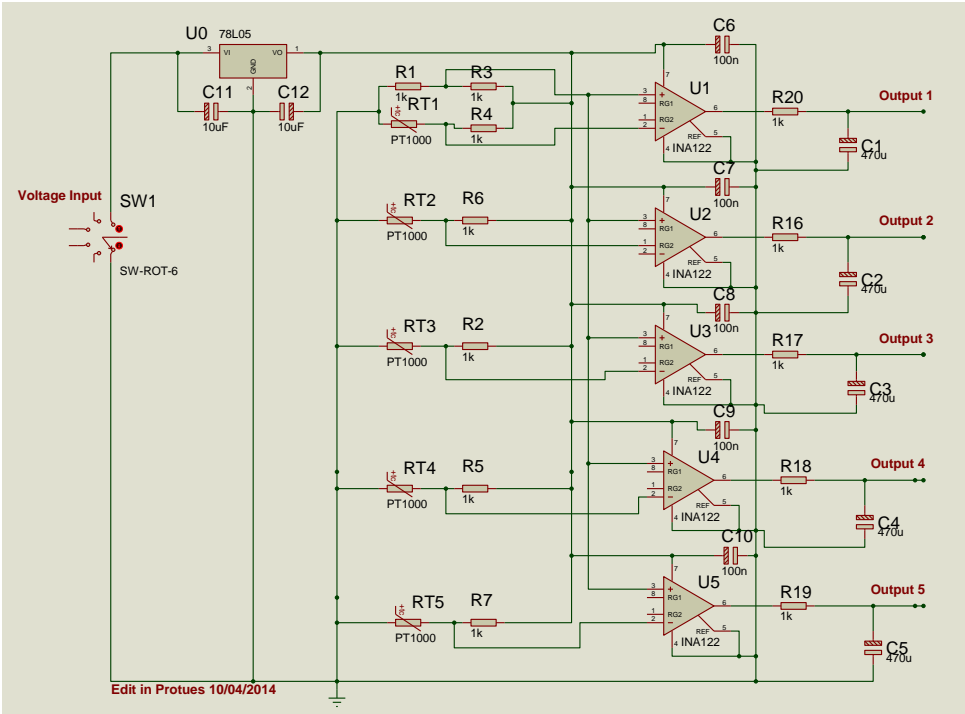


Fig. 3.6: Temperature measurement PCB

As each PCB just has 5 channels, we need 2 PCBs for this experiment.

Fig. 3.7 presents one of the PCB entities,

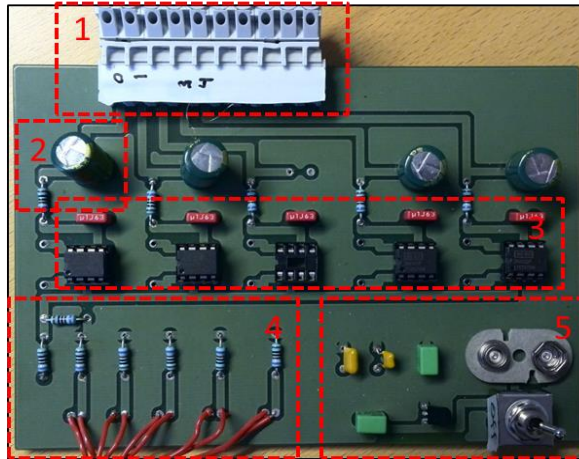


Fig. 3.7: The PCB entity

Each part corresponds to the one in schematic circuit drawn by PROTUES.

- Part 1: output ports which will connect to the LabVIEW
- Part 2: low-pass filter circuit
- Part 3: amplifier circuit
- Part 4: Wheatstone bridges
- Part 5: voltage input and three terminal regulator (78L05)

After the introductions of all the function blocks above, an overall temperature measurement system can be presented as follows,

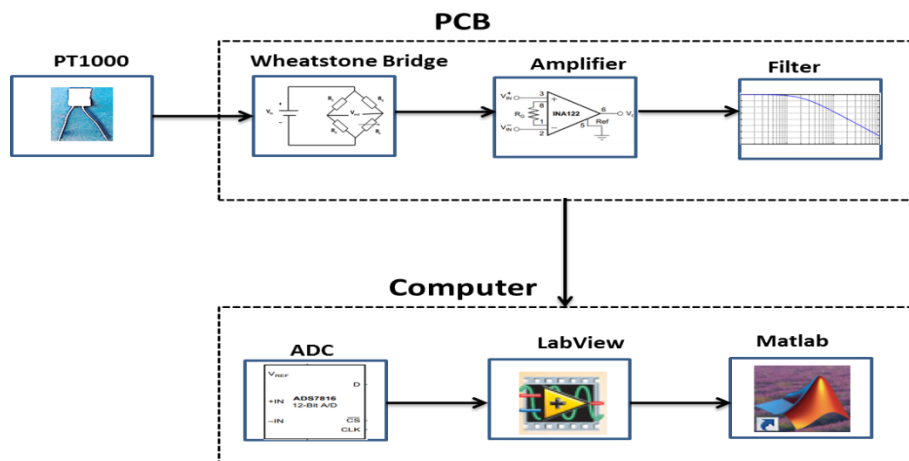


Fig. 3.8: The overall diagram of the temperature measurement system

3.3 Data handling system

3.3.1 LabVIEW

In this part, the software LabVIEW will be used to accomplish the task of acquiring data. LabVIEW (Laboratory Visual Instrument Engineering Workbench) is a system-design platform and development environment for a visual programming language designed by National Instruments (NI). For communicating with the data acquisition hardware, a DAQmx Assistant will be needed at the software. This tool helps us to create the necessary applications without programming through a graphical interface for configuring both simple and complex data acquisition tasks. Fig. 3.8 shows the block diagram in which a DAQmx, 8 channels have been designed. The data acquired in each period from the channels through the hardware will be calculated by the block MEAN. So the average values will be shown in the front panel, see Fig. 3.9.

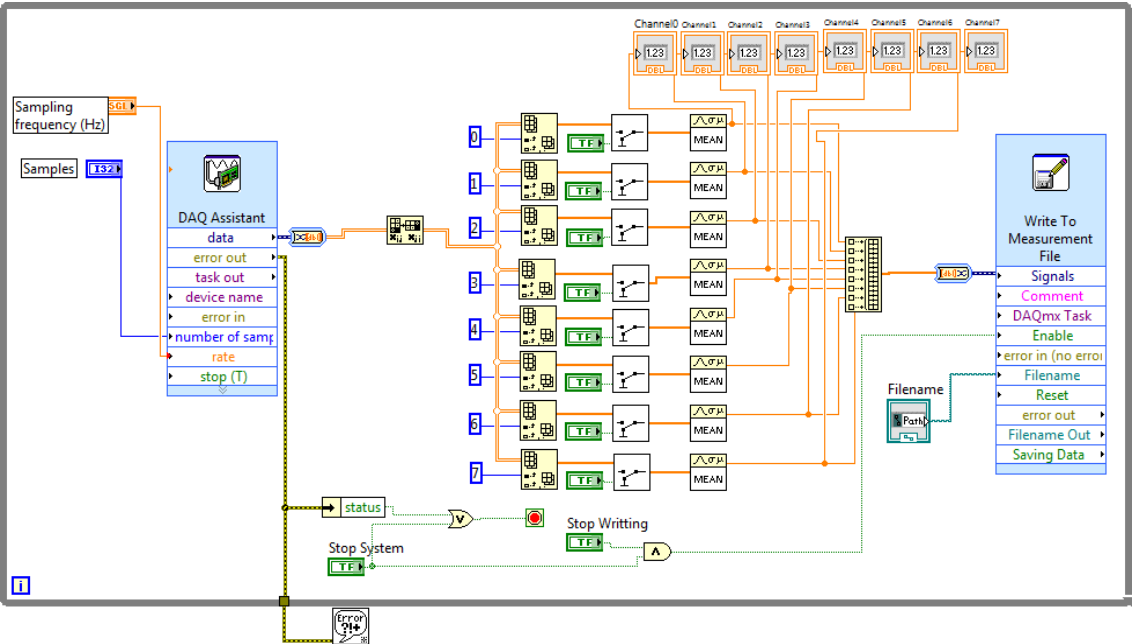


Fig. 3.8: The Block Diagram in LabVIEW

In order to make the data acquisition proceed continuously, it needs also a circulation While-Loop that means it will keep running until the stop button is pressed. Eventually the acquired data will be saved into the file under the format of Text or Binary.

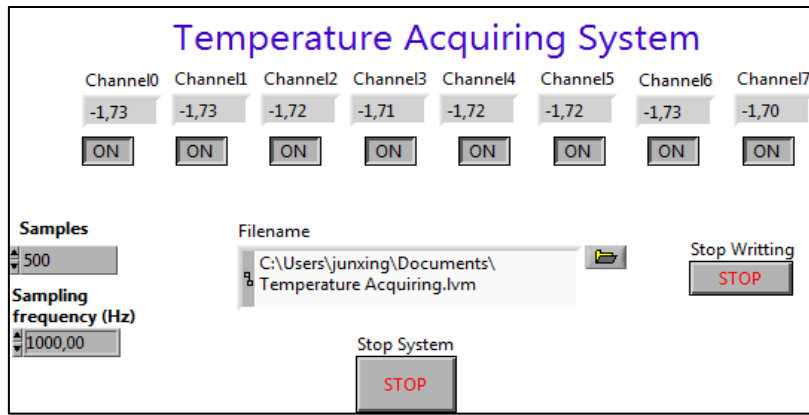


Fig. 3.9: The Front Panel in LabVIEW

As visualized in Fig. 3.9, the sample frequency has been set to be 1000Hz, which means that each iteration 1000 acquisition operations will be executed. The sample makes an average among the number of samples obtained from each channel.

Table 3.5 shows the voltages in each channel corresponding to sampling data from 30°C to 130°C.

Table 3.5: The sampling data from LabVIEW

Reference Temperature [°C]	Ch0 [V]	Ch1 [V]	Ch2 [V]	Ch3 [V]	Ch4 [V]	Ch5 [V]	Ch6 [V]	Ch7 [V]
33.1	0.752134	0.753633	0.751973	0.751978	0.751934	0.752539	0.747778	0.756914
34.5	0.787563	0.791045	0.789619	0.786597	0.786685	0.788032	0.785068	0.790898
38.8	0.873174	0.874209	0.873613	0.871563	0.872803	0.874014	0.869365	0.875879
41.8	0.947227	0.947349	0.947173	0.946519	0.944292	0.947202	0.942783	0.950176
46	1.027930	1.029731	1.025635	1.025474	1.026299	1.029204	1.022666	1.030469
49.7	1.098652	1.100083	1.098579	1.097563	1.098364	1.098931	1.094146	1.101436
54.3	1.186265	1.187134	1.186328	1.184722	1.186094	1.188286	1.181816	1.187939
58.4	1.259897	1.262368	1.260190	1.259814	1.259800	1.261021	1.256865	1.264585
64.8	1.380786	1.382109	1.380093	1.377852	1.379082	1.381895	1.376997	1.384492
68.7	1.450229	1.450737	1.450073	1.450117	1.450405	1.450815	1.445552	1.455293
75.6	1.577217	1.578608	1.576934	1.576548	1.577134	1.578018	1.572349	1.581655
80	1.660117	1.660859	1.659600	1.658047	1.659077	1.660298	1.655020	1.661333
84.5	1.733564	1.735991	1.733379	1.731865	1.733174	1.734990	1.728750	1.737354
89.3	1.816421	1.816914	1.816318	1.816006	1.816323	1.816914	1.811943	1.820273
94.7	1.904121	1.904409	1.903745	1.902715	1.903877	1.904468	1.899585	1.908921
99.6	1.987808	1.991250	1.987490	1.987212	1.987563	1.990415	1.982954	1.992173
104.3	2.060552	2.061694	2.060493	2.060571	2.060630	2.063604	2.057671	2.065679
109.8	2.148716	2.151567	2.148555	2.148452	2.148765	2.152139	2.146699	2.153462
114	2.211089	2.212051	2.210371	2.209697	2.211357	2.212104	2.207148	2.216309
120	2.316572	2.319150	2.315112	2.314834	2.315957	2.319150	2.313838	2.321147
125.5	2.402100	2.402432	2.402070	2.401514	2.402134	2.402681	2.397871	2.406221
129	2.445713	2.446514	2.444619	2.445117	2.446001	2.446685	2.441489	2.451016

In order to reflect the relationship between the output voltage in each channel and the temperature, some mathematical transformations are necessary. From (3.8) we know the amplification factor equals 5, so (3.6) can be transferred into

$$R_t = \frac{4.93 + 2 \frac{V_{channel}}{5}}{4.93 - 2 \frac{V_{channel}}{5}} * 1000 \quad (3.16)$$

where the constant 4.93 is the voltage output from the three terminal regulator $78L05$, $V_{channel}$ is the voltage of each channel. The constant 1000 is the resistance of R_1 , R_2 and R_3 in the Wheatstone bridge.

Then the temperature equation based on (3.4) can be shown as follows,

$$t = \frac{-1000A + \sqrt{(1000A)^2 - 4 * 1000B(1000 - R_t)}}{2 * 1000B} \quad (3.17)$$

where the constant 1000 is the value of R_0 for the PT-1000 sensor, $A = 3.9080 * 10^{-3}$, $B = -5.8019 * 10^{-7}$.

3.3.2 Calibration

The device performance can change over time. For example a zero-drift error occurs in the amplifier circuit. So the measurement results will not correspond to the theoretical ones exactly. In order to put the accuracy to the test, the precision and the repeatability within the specification limits of the data acquisition system, the procedure of calibration is a must [15].

The first important factor to this procedure is the creation of an environment with homogeneous temperature. At the same time, a temperature measurement instrument will be used, as a reference. All the results measured in any other channel will refer to this value. Fig. 3.10 (a) shows the thermometer FLUKE 489 that can display the temperature directly with a thermocouple probe in this experiment.

Then all the PT-1000 sensors along with the thermocouple will be placed into the same test environment. The test temperature will vary from 200°C to 20°C within an arbitrary interval. The voltage levels of each channel and the temperature of the thermometer are registered. Dealing with the data in Matlab, we can obtain a mathematical temperature function ($T = f(v)$) curve for each channel exclusively.

As heating source, 3 possibilities are proposed as below,

- Water in the pan
- Halogen lamp
- Canola oil in the oil bath

The first method can be approached easily because its needed medium is water. But the big drawback is that the boiling point for water is 100°C, we cannot calibrate the sensors above 100°C with the same procedure. Moreover, it is necessary to control the depth of the sensors immersed in the water for the reason that water is a conducting medium.

The second method is visualized in Fig. 3.10 (b). Ideally, the halogen lamp can create an ambient with the temperature above 100°C, but the temperature inside is not exactly homogeneous. Highest in the center and then attenuated gradually with the increase of distance to the center. The most important point is that during the measurement, the temperature increases so slowly that some plastic cover protections of the sensor begin to melt before the temperature reaches 200°C.

The third method refers to Fig. 3.10 (c) is the final one taken in this test. It combines the advantages of the first and the second method. All the sensors will be immersed in the Canola oil, whose boiling point exceeds 300°C. Canola oil is also an excellent insulating medium and it has been used as insulation oil in Toshiba transformers.

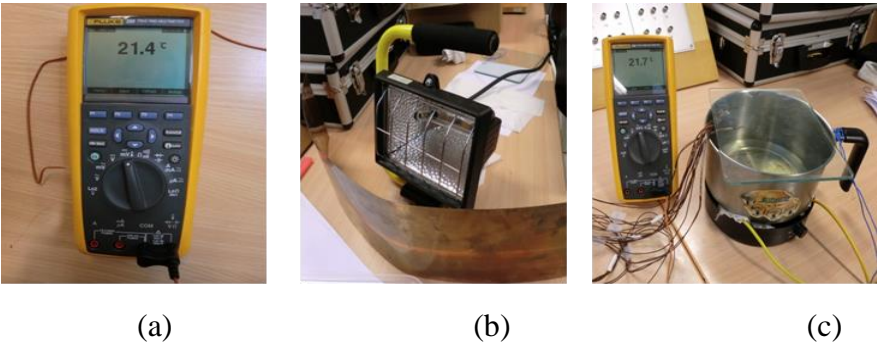


Fig. 3.10: (a) FLUKE thermometer, (b) Halogen lamp test method, (c) Canola oil in the oil bath test method.

Fig. 3.11 presents the whole calibration system in this experiment.

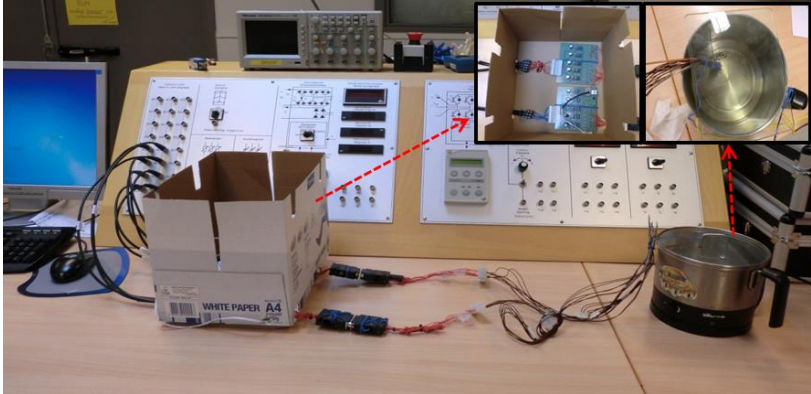


Fig. 3.11: The calibration system

3.3.3 Matlab

In this part, the data registered by LabVIEW will be implemented in Matlab. Fig. 3.12 shows the function of temperature and voltage for Channel 0. The abscissa stands for voltage and the ordinate represents temperature. The fitting curve is drawn by $Fitch0=fit(ch0, Tem, 'poly2')$ c.f Appendix [B] in Matlab. Obviously the fitting curve matches strictly the theoretical curve in the temperature range which we need during this test (from 30°C to 125°C). Besides the calibration points match the fitting curve properly and a quadratic function is given which is only valid for the associated channel. In this case, the quadratic function for Channel 0 is presented as follows,

$$T_0 = 5.578V^2 + 38.83V + 0.4455 \quad (3.18)$$

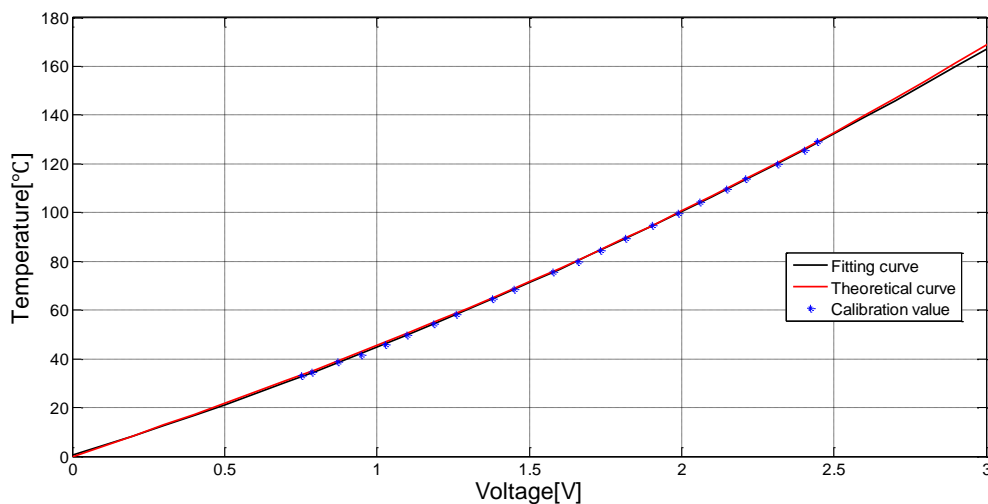


Fig. 3.12: $T=f(V)$ for Channel 0

Chapter 4

4. Manufacture procedure

4.1 Materials for the construction of transformer

As it has been mentioned before, the aim of this work is to measure the thermal resistances of the transformer and then compare them with the theoretical ones. In order to make sure that the measured and theoretical values match each other perfectly, several models with different parameters and thermal insulation materials will be constructed.

Generally, for each model, some necessary components are the same, e.g. coil former, core, PT-1000 sensors, copper wire and thermal insulation tape etc. Fig. 4.1 shows the main parts of the model.

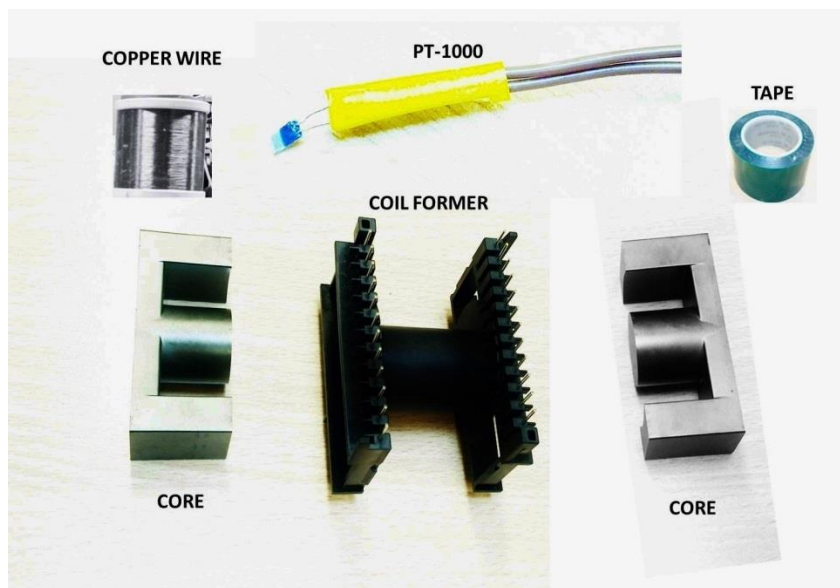


Fig. 4.1: The main components for each model

The PT-1000 sensor is used to measure the temperature of each specified point and the tape is for increasing the interlayer thermal resistance. Besides, some other auxiliary components to facilitate the experiment are needed. Table 4.1 shows the list of the necessary devices during the test.

Table 4.1: The bill of the needed materials

Product	Model	Specification
Coil-former	CPH-ETD59-1S-24P	[Fig. 4.2]
Core	ETD59	[Fig. 4.3]
PT-1000	Heraeus FK422 PT-1000 B	[Appendix A]
Copper wire	BELDEN 8053	$\varnothing=0.4$ mm
Insulation tape	TESA - 50600-00001-00	[Fig. 4.4]
Heat Transfer Compound	Electrolube HTS35SL	$k=0.9$ W/m.K
Thermal camera	FLIR i7	-

where k is the thermal conductivity, \varnothing is the diameter of the copper wire.

4.2 Characteristic parameters of the materials

For calculating the theoretical thermal resistance, we need to know the characteristic parameters of each relevant material. Fig. 4.2 illustrated the dimensions of the ETD-59 coil former.

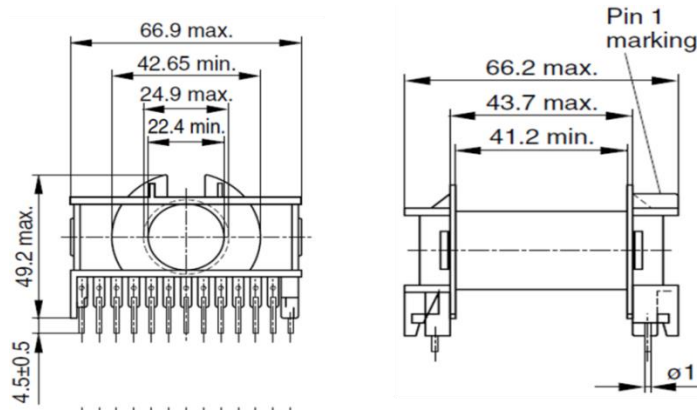


Fig. 4.2: The dimension of ETD 59 coil former

The three most important dimensions of the coil former in this work are the length (41.2mm), the external diameter (24.9mm) and the internal diameter (22.4mm).

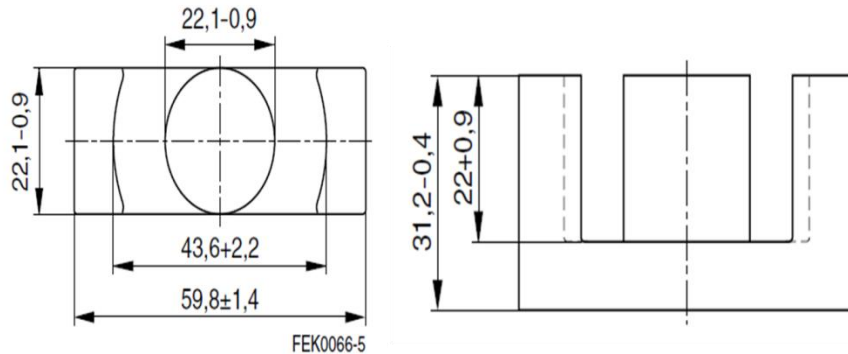


Fig. 4.3: The dimensions of ETD 59 core

Fig. 4.3 shows the detail of the core ETD 59. By comparing it with Fig. 4.2 we can observe that the diameter of the cylindrical central leg (22.1-0.9mm) does not equal the bobbin's internal diameter, which means that there are some air gaps between the two assembly units. In order to eliminate the influence brought by the air, several layers of tape with known heat conductivity will be wrapped to the core. Fig. 4.4 lists the main characteristics of the thermal insulation tape.

Technical Data			
■ Backing material	PET	■ Elongation at break	110 %
■ Type of adhesive	silicone	■ Tensile strength	72 N/cm
■ Total thickness	80 μ m	■ Temperature resistance	220 °C
■ Adhesion to steel	4 N/cm		

Fig. 4.4: The main parameters of the thermal insulation tape

The manufacturer does not provide its heat conductivity, but we can use an approximate value $k=0.15\text{W/m.k}$ for the tape since its backing material is PET [16]. Besides, its temperature resistance is up to 220°C, which is sufficient for the test.

4.3 Transformer construction

In this subsection, a short description of the manufacture procedure and the position of the PT sensors in the transformer will be given.

All the tested transformers in this work consist of 5 layers and needs 8 PT sensors totally. For the first test, there will not be any interlayer thermal insulation tape, which differs from the second one. But the positions of the PT sensors during two tests are the same.

Table 4.2 shows the positions of the PT sensors in the transformer as well as their labels.

Table 4.2: Position and mark for each PT sensor

PT	Position	Mark
1	Under layer 1	T1
2	Under layer 2	T2
3	Under layer 3	T3
4	Under layer 4	T4
5	Under layer 5	T5
6	On the surface of layer 5	TY
7	On the surface of the core or coil former	TC
8	Outside the transformer	TA

For clearer reason, the positions of the PT sensors are visualized in Fig. 4.5 and Fig. 4.6 from top view and side view respectively.

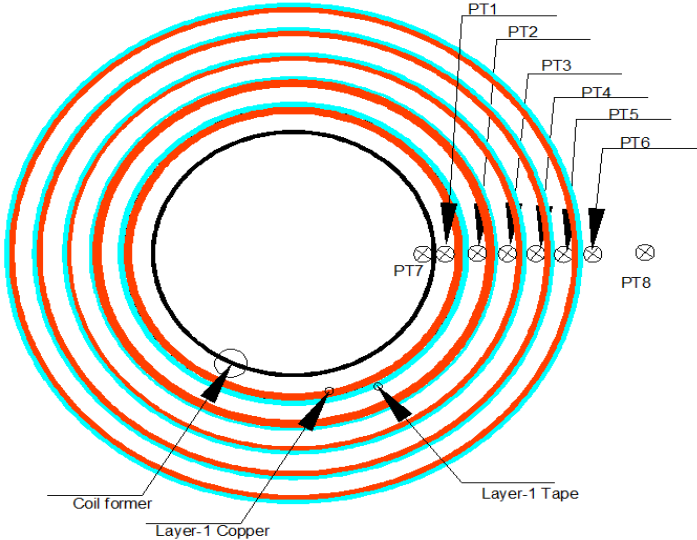


Fig. 4.5: Position of the PT sensors in the transformer, top view

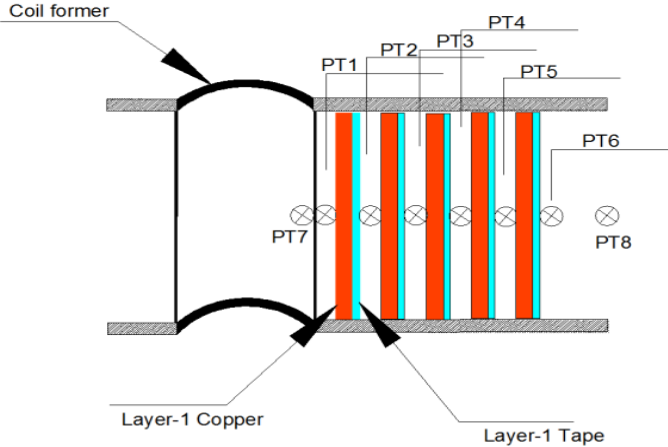


Fig. 4.6: Position of the PT sensors in the transformer, side view

In test 2, the thermal resistance between the first layer and the ferrite core R_{thC1} will be decided, so the position of PT7 differs from the previous ones. Fig. 4.7 illustrates the schematic when the core is plugged into the coil former.

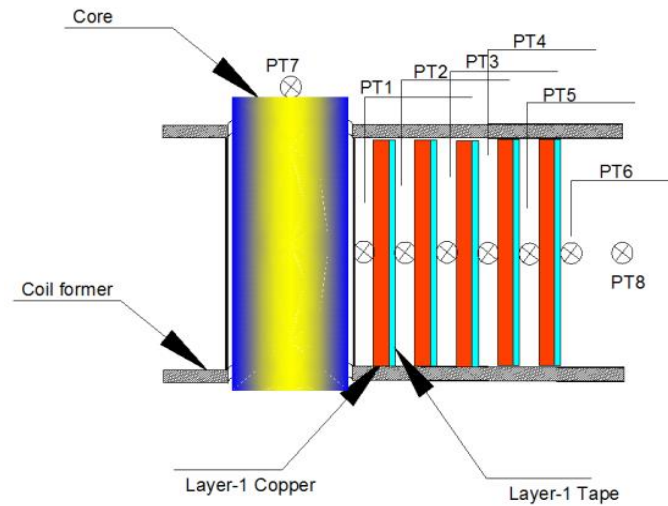


Fig. 4.7: Position of the PT sensors in the transformer, side view with core

4.3.1 Construction step

In this section the procedure of construction will be explained. Even though several different models will be made, the principal manufacture procedures are the same.

STEP 1: Choose the appropriate copper wire. The larger copper's diameter that is chosen, the smaller its steady state resistance will be. It can lead to a bigger error during the calculation of how much energy is dissipated in the windings. In this case, copper with a diameter of 0.4mm will be chosen. Then we fix the coiling tool on the table and keep the wire tense enough to make sure all the coils are placed next to each other properly. In addition, the length of the copper in each layer should be recorded which is needed in the theoretical part. This step is visualized in Fig. 4.8.



Fig. 4.8: Choosing and wrapping the copper wire

STEP 2: The placing of the PT sensors. As the chosen sensor has not any protection, the PT element will be broken easily when the copper wire is too big. Besides, in order to ensure the accuracy measurement, all the interlayer PT sensors should be placed in the same longitudinal vertical plane. Fig. 4.9 shows the PT element and its placement.

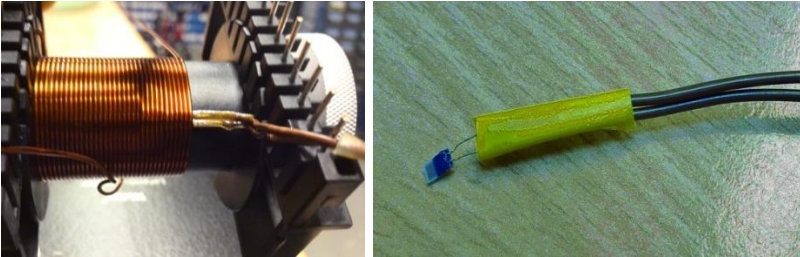


Fig. 4.9: The placing of PT sensors

STEP 3: As the round conductor is chosen, there will be some air pockets between each coil and each layer. Fig. 4.10 displays the precise positions of the air pockets.

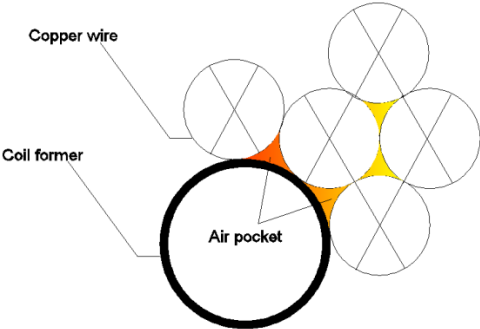


Fig. 4.10: Air pockets in the transformer winding

The thermal conductivity of air is about 0.03 W/m.k , which can produce a large and uncertain thermal resistance. So it is necessary to fill in the porosity with some grease. Fig. 4.11 shows the winding covered by the heat transfer compound with a heat conductivity of 0.9 W/m.k . This measure can reduce as much as 75% of the thermal contact resistance [17]. Under this condition, the porosity and thermal contact resistance can be negligible.

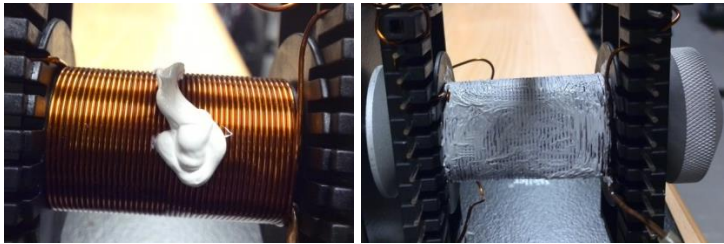


Fig. 4.11: Grease on the surface of each winding

STEP 4: When the fifth layer is finished, a layer of electrical insulation tape will be wrapped on to the winding's surface. Then all the PT sensors wires are welded to the metal terminals of the coil former. Fig. 4.12 illustrates the final assembly model.

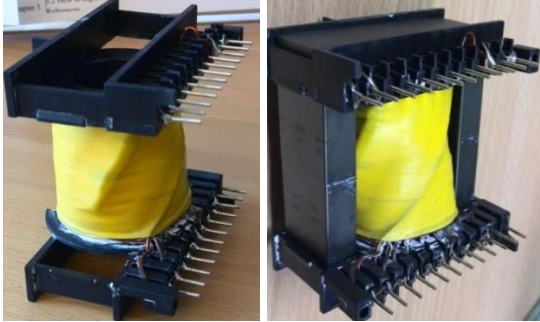


Fig. 4.12: Final assembly unit

Chapter 5

5. Experiment set-up and test analysis

5.1 Experiment set-up

5.1.1 Thermal model

The previous chapter has introduced the construction procedure of the transformer. In this part, the thermal model and its verification will be presented.

To a normal operating AC transformer, the power dissipation is the result of Joule loss, hysteresis loss and eddy loss. Most losses produced by the windings dissipate directly into the air, a small percentage of them go through the core and then dissipate. To the core, it has the similar heat transportation. According to the theory of heat-electricity analogy, the difference in temperature, heat flow and thermal resistance can be regarded as the voltage or potential difference, current and electric resistance respectively. So a lumped heat model as Fig. 5.1 can be presented.

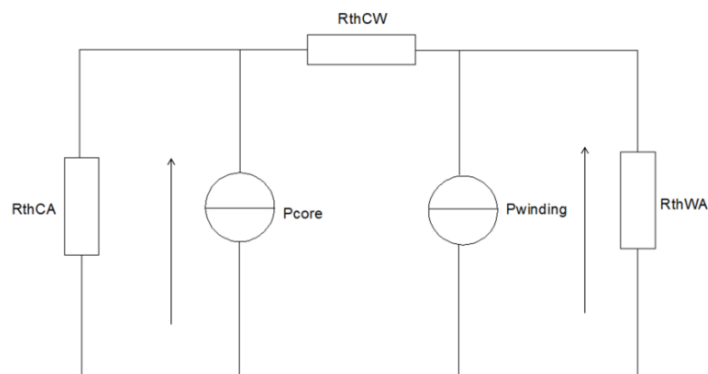


Fig. 5.1: Lumped heat model

where the windings' loss $P_{winding}$ and the core's loss P_{core} are considered as two independent thermal excitation resources. R_{thCA} and R_{thWA} represent the thermal resistance between the core and the air, the windings and the air respectively.

When the three thermal resistances are determined, we can derive the relationship between the temperature and the conducted current without placing any temperature sensor.

Based on Fig. 5.1, the heat network shown in Fig. 5.2 can be deduced for a 5-layer AC transformer.

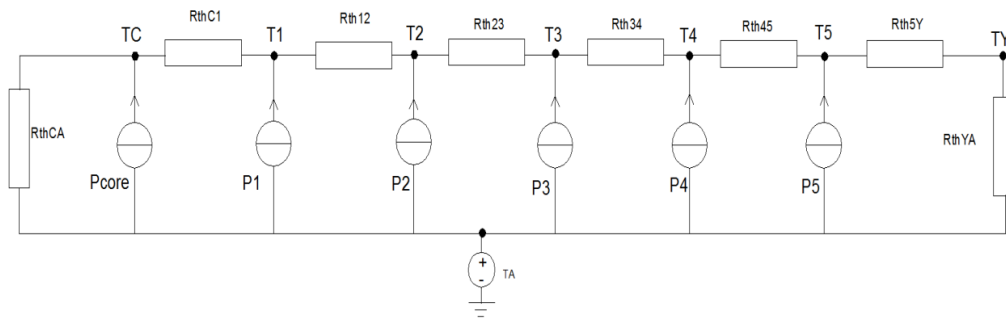


Fig. 5.2: 5-layer transformer heat network

Table 5.1 shows the meaning of all the signs from Fig. 5.2.

Table 5.1: Meaning of the signs

Sign	Meaning	Sign	Meaning	Sign	Meaning
T1	Temperature of layer 1	P1	Heat flow of layer 1	RthCA	Thermal resistance between core and ambient
T2	Temperature of layer 2	P2	Heat flow of layer 2	RthC1	Thermal resistance between core and layer 1
T3	Temperature of layer 3	P3	Heat flow of layer 3	Rth12	Thermal resistance between layer 1 and layer 2
T4	Temperature of layer 4	P4	Heat flow of layer 4	Rth23	Thermal resistance between layer 2 and layer 3
T5	Temperature of layer 5	P5	Heat flow of layer 5	Rth34	Thermal resistance between layer 3 and layer 4
TY	Surface temperature on layer 5	P _{core}	Heat flow of the core	Rth45	Thermal resistance between layer 4 and layer 5
TA	Ambient temperature			Rth5Y	Thermal resistance between layer 5 and its surface
TC	Core temperature			RthYA	Thermal resistance between ambient and surface of layer 5

In this work, in order to determine the thermal resistance, all the tests will be conducted with DC supply, so that P_{core} will not exist anymore, Fig. 5.2 can turn to be,

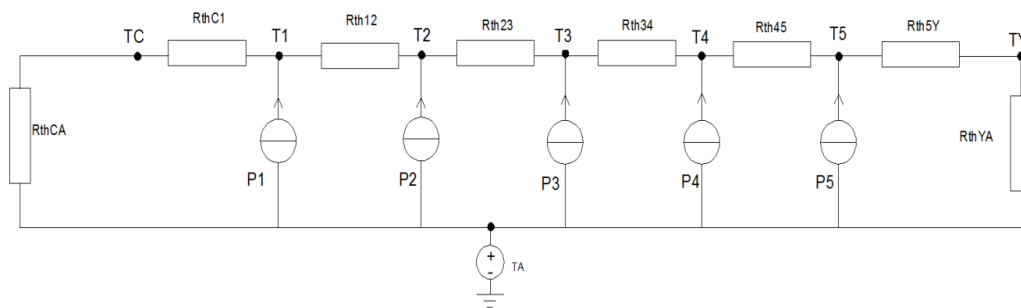


Fig. 5.3: 5-layer transformer heat network without core loss

5.1.2 Determination of the excitation resource P

For each layer, the heat dissipation is expressed thanks to the Joule principle $P=I^2R$. The currency can be read through an ampere meter. For the resistance, nevertheless, it will be a bit more complicated as it varies when the temperature changes. Suppose that we have a length of 20m copper wire with a diameter of 0.85mm, its resistance coefficient at 20°C is $\rho=1.68 \times 10^{-8} \Omega \cdot m$ and its temperature coefficient is $\alpha = 0.003862 k^{-1}$. According to (2.9), we can calculate its resistance $R_0=0.6\Omega$. When the temperature rises up to 100 °C, its resistance becomes 0.78 Ω which means that it has changed about 31%. As the temperature of each layer is so close, for simple reason, they can be considered to be equal; when the total power is read by the power meter, the length of each layer will be the unique factor to decide each layer's heat dissipation. Fig. 5.2 shows the length and the rate of each layer for test 1.

Table 5.2: The length and the rate of each layer

Layer NO.	Length(m)	Rate
1	3.73	17%
2	4.05	19%
3	4.14	19%
4	4.45	21%
5	4.94	23%
total	21.3	100%

5.2 Test 1- No interlayer thermal insulation

In this test, there is not any thermal tape between each layer. To stop the outside air flow and make a balanced temperature without any fluctuation, the tested model is put into a plastic chamber which is visualized in Fig. 5.4.

5.2.1 External heating source

In the first phase, a power resistor is put inside the coil former to act as the heating source; when the outside of the coil former is wrapped with thermal insulation material, all the heat dissipates through the windings. This heat transport can be regarded as just one dimensional.

Fig. 5.5 shows the schematic of the heat flow. Then the resistor is conducted with different DC power (about 1W, 2W, 3W) to get an average value.



Fig. 5.4: Test without interlayer thermal insulation

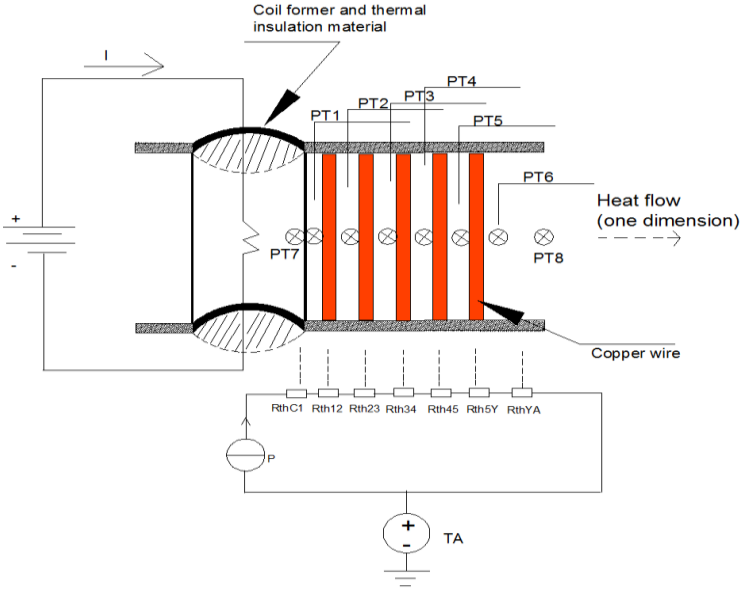
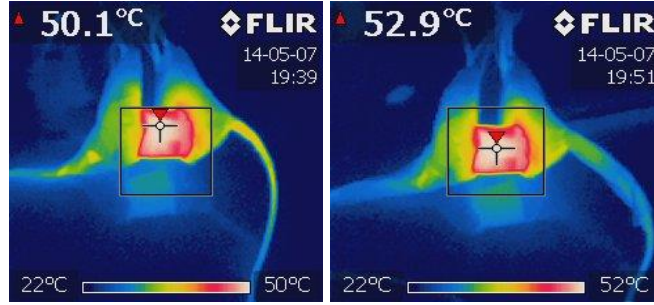


Fig. 5.5: Tested model with external heat resource

In order to ensure the thermal insulation effect is good enough, we can use a thermal camera to examine the outside temperature of the tested model. Fig. 5.6 shows the thermal images captured by a FLIR i7 thermal camera.



(a)



(b)

(c)

Fig. 5.6: (a) FLIR i7 thermal camera (b) Primal thermal insulation (c) Improved thermal insulation

Based on Fig. 5.5, the thermal resistances can be derived as

$$R_{thC1} = \frac{T_c - T_1}{P} \quad (5.1)$$

$$R_{th12} = \frac{T_1 - T_2}{P} \quad (5.2)$$

$$R_{th23} = \frac{T_2 - T_3}{P} \quad (5.3)$$

$$R_{th34} = \frac{T_3 - T_4}{P} \quad (5.4)$$

$$R_{th45} = \frac{T_4 - T_5}{P} \quad (5.5)$$

$$R_{th5Y} = \frac{T_5 - T_Y}{P} \quad (5.6)$$

$$R_{thYA} = \frac{T_Y - T_A}{P} \quad (5.7)$$

By applying Matlab, the relationship between temperature and measured times can be illustrated in curves. Fig. 5.7 shows the response of the temperature of each part from an original ambient temperature when the power resistor is conducted with $P=3.865W$.

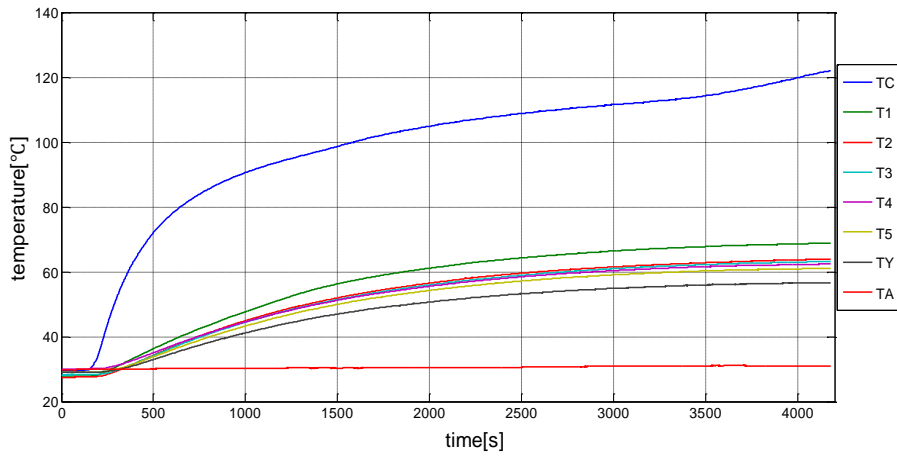


Fig. 5.7: Experimental temperature measurement with $P=3.865W$

Fig. 5.8 and Fig. 5.9 show the temperature response when the power is reduced to $P=2.403W$ and $P=1.680W$ respectively. So their curves have a descending tendency.

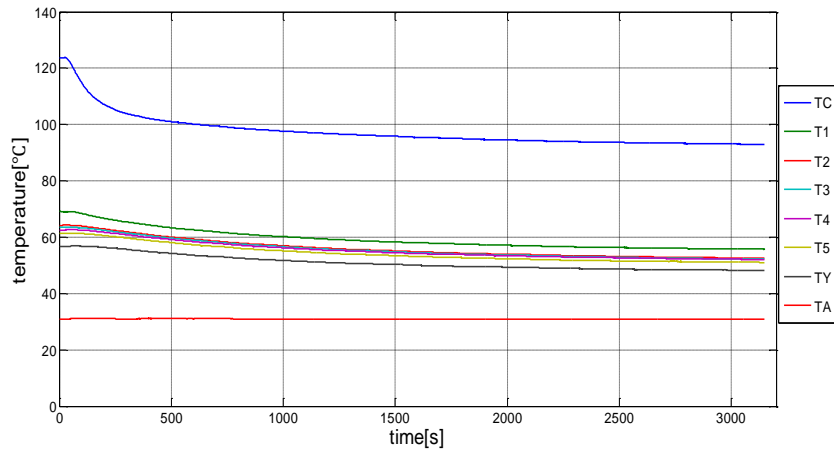


Fig. 5.8: Experimental temperature measurement with $P=2.403W$

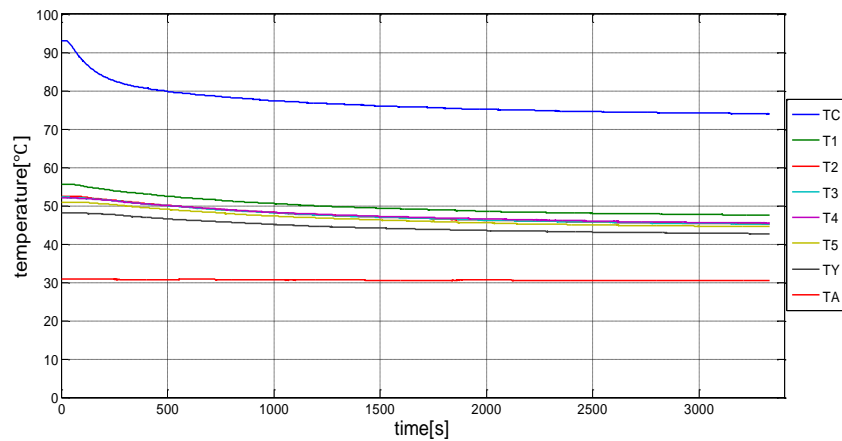


Fig. 5.9: Experimental temperature measurement with $P=1.680W$

Table 5.3 shows the temperature of each PT sensor and their variations in different power.

Table 5.3: Temperature versus different power

No.	P(W)	T1(°C)	T2(°C)	T3(°C)	T4(°C)	T5(°C)	TY(°C)	TC(°C)	TA(°C)
1	3.865	68.92	63.97	63.20	62.41	61.08	56.67	121.98	30.96
2	2.403	55.72	52.62	52.21	52.08	51.04	48.14	92.97	30.87
3	1.680	47.48	45.27	45.18	45.49	44.54	42.68	73.93	30.49

Combining Table 5.3 and (5.1) to (5.7), the thermal resistances can be calculated in Table 5.4.

Table 5.4: Thermal resistance versus different power

No.	Rth_total (°C/w)	RthC1 (°C/w)	Rth12 (°C/w)	Rth23 (°C/w)	Rth34 (°C/w)	Rth45 (°C/w)	Rth5Y (°C/w)	RthYA (°C/w)
1	23.551	13.73	1.28	0.20	0.20	0.35	1.14	6.65
2	25.838	15.50	1.29	0.17	0.06	0.43	1.21	7.18
3	25.853	15.74	1.32	0.05	-0.18	0.56	1.11	7.26
Mean	25.081	14.99	1.30	0.14	0.03	0.45	1.15	7.03

Fig. 5.10 to Fig. 5.12 illustrate the variation tendency of the thermal impedance, but no matter how the power changes, the thermal impedance can trend to a similar value at steady state, which proves that thermal resistance depends on the characteristics of the object rather than the outside excitation.

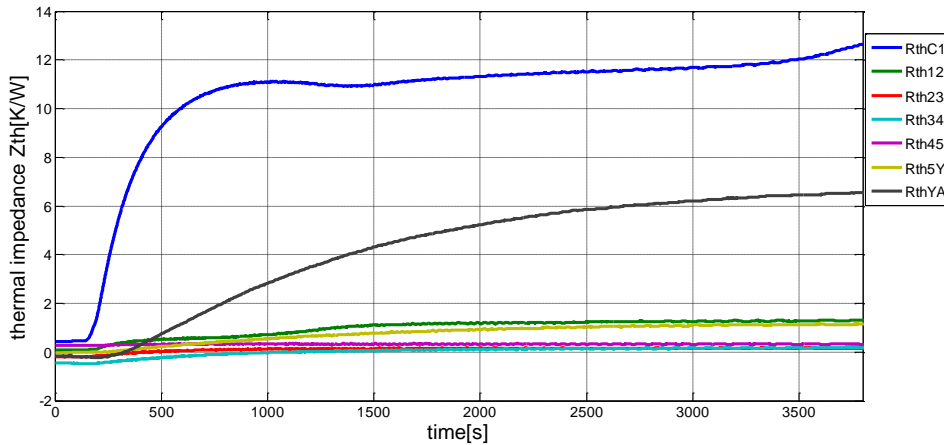


Fig. 5.10: Experimental thermal impedance measurement with $P=3.865W$

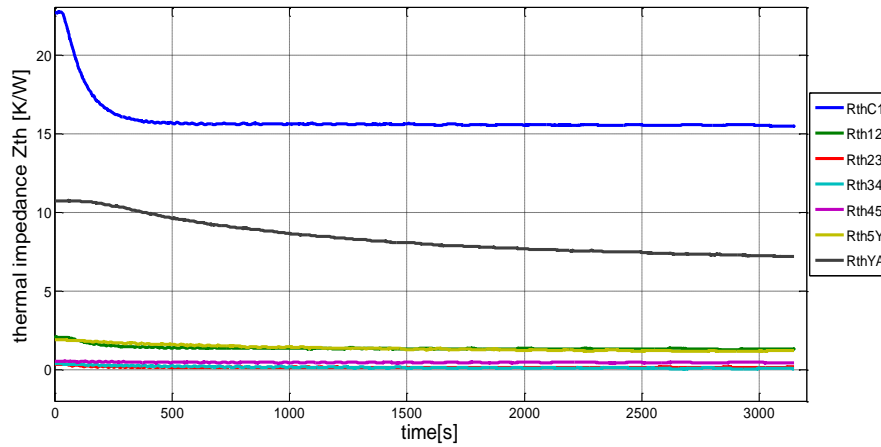


Fig. 5.11: Experimental thermal impedance measurement with $P=2.403W$

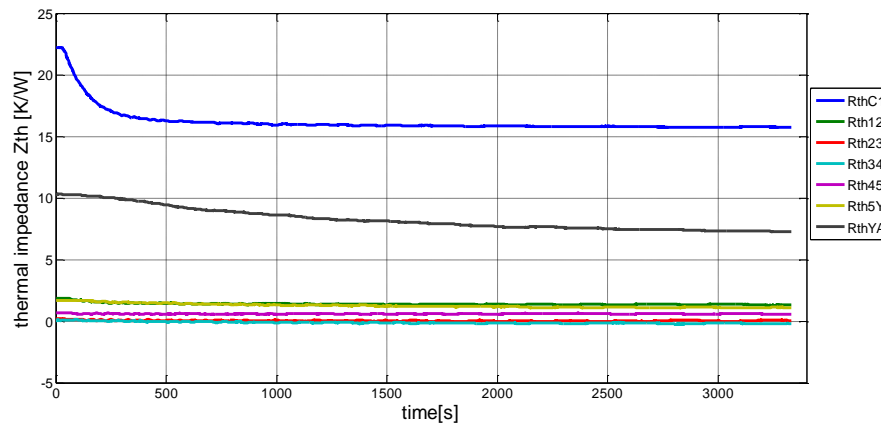


Fig. 5.12: Experimental thermal impedance measurement with $P=1.680W$

5.2.2 Internal heating source

In the first phase, the thermal resistances have been calculated from the measured temperatures. Based on the thermal resistances, the temperature of each point can be predicted. When the temperature measurement in this phase is done, the comparison between the theoretical and measured values can be made.

Fig. 5.13 shows the winding directly connected with a DC supply to simulate the real operating situation.

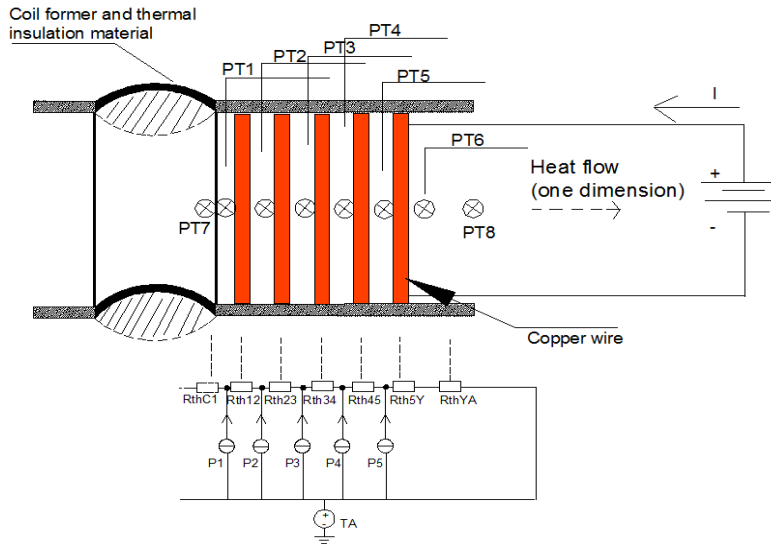


Fig. 5.13: Tested model with internal heat resource

As the heat flow merely goes through the winding, theoretically there is no heat dissipating from the core. So R_{thC1} does not exist in this test.

For the calculation of the heat network, the Mesh-Current-Analysis can be applied [18]. Fig. 5.14 shows the whole 'Mesh' and the imagined 'Mesh Currencies' $PL1$ to $PL5$ which mean the heat flow in each 'Mesh'.

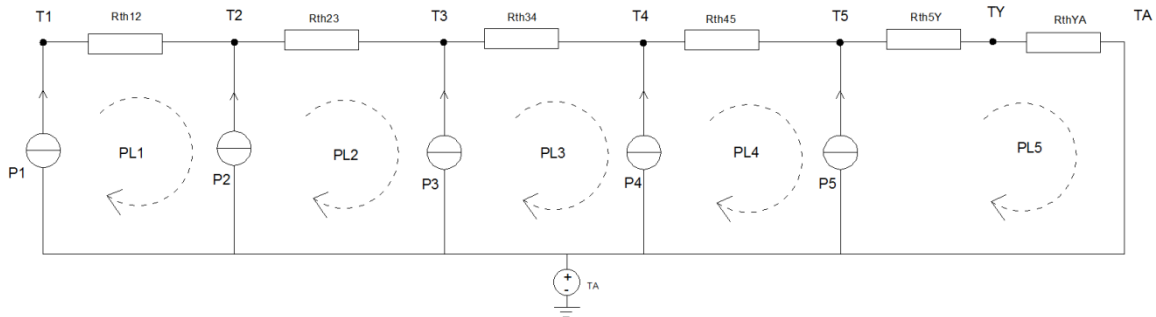


Fig. 5.14: Mesh-Current-Analysis for the heat network

In Fig. 5.14, there are six to-be-solved temperatures, but only five constraint equations can be established, so an additional equation between $T5$ and TY will be added.

Based on Fig. 5.14, the relevant equations can be deduced as

$$R_{th12} * PL1 = T1 - T2 \quad (5.8)$$

$$R_{th23} * PL2 = T2 - T3 \quad (5.9)$$

$$R_{th34} * PL3 = T3 - T4 \quad (5.10)$$

$$Rth45 * PL4 = T4 - T5 \quad (5.11)$$

$$(R5Y + RYA)PL5 = T5 \quad (5.12)$$

$$PL1 = P1 \quad (5.13)$$

$$PL2 = PL1 + P2 \quad (5.14)$$

$$PL3 = PL2 + P3 \quad (5.15)$$

$$PL4 = PL3 + P4 \quad (5.16)$$

$$PL5 = PL4 + P5 \quad (5.17)$$

Then the solution for temperature can be,

$$T1 = T2 + R12 * PL1 \quad (5.18)$$

$$T2 = T3 + R23 * PL1 \quad (5.19)$$

$$T3 = T4 + R34 * PL1 \quad (5.20)$$

$$T4 = T5 + R45 * PL1 \quad (5.21)$$

$$T5 = (R5Y + RYA) * PL5 \quad (5.22)$$

$$TY = RYA * PL5 \quad (5.23)$$

When the winding is conducted with different powers, the measured and model-check results are demonstrated as Table 5.5 and Table 5.6 respectively.

Table 5.5: Measured results

No.	P(W)	T1(°C)	T2(°C)	T3(°C)	T4(°C)	T5(°C)	TY(°C)	TA(°C)
1	2.815	55.28	55.96	55.94	55.67	54.73	51.21	30.67
2	7.983	99.78	101.84	101.40	99.19	97.41	86.83	31.91
3	12.062	134.23	137.11	136.64	133.68	130.60	113.22	33.10

Table 5.6: Model-check results

No.	P(W)	T1(°C)	T2(°C)	T3(°C)	T4(°C)	T5(°C)	TY(°C)	TA(°C)
1	2.815	55.49	54.71	54.71	54.66	53.70	50.46	30.67
2	7.983	102.31	100.49	100.09	99.97	97.24	88.04	31.91
3	12.062	139.46	136.73	136.11	135.94	131.81	117.91	33.10

In order to compare the difference between the measured and theoretical values, the curve of each temperature is illustrated as Fig. 5.15, Fig.5.16 and Fig. 5.17.

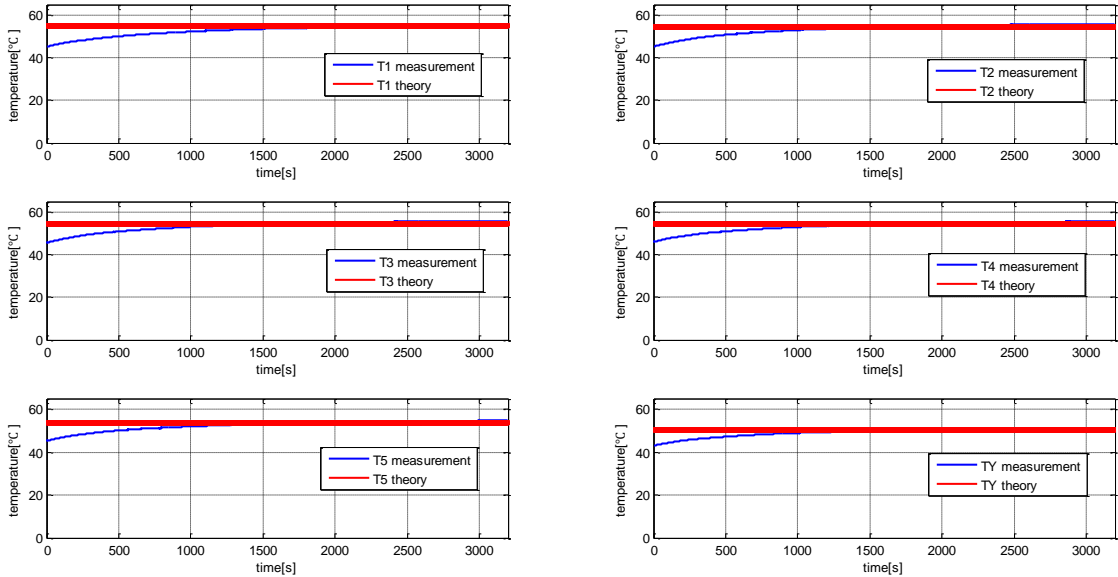


Fig. 5.15: Temperature difference of each point with $P=2.815W$

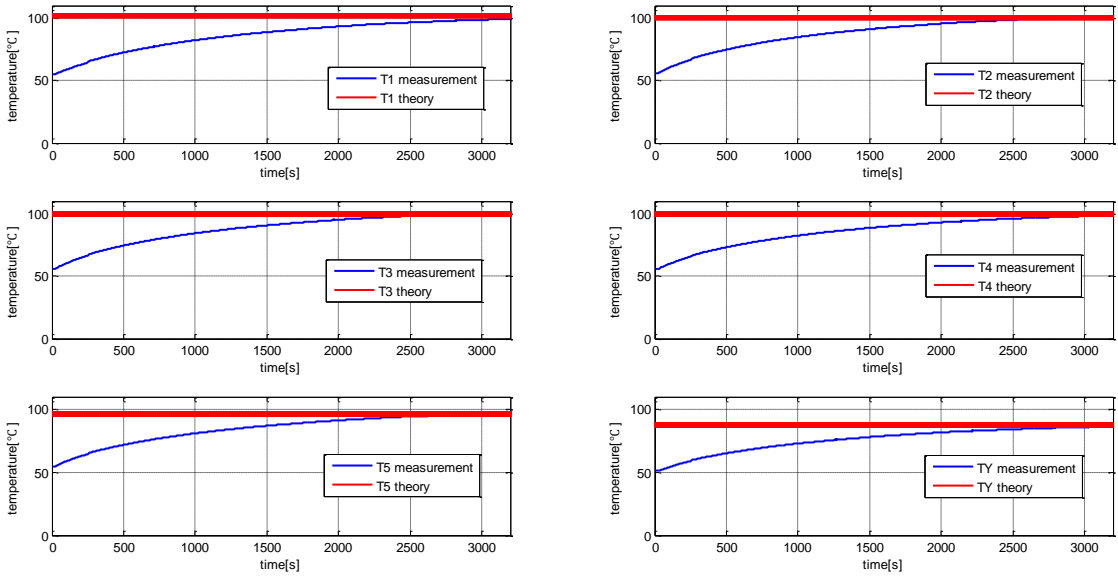


Fig. 5.16: Temperature difference of each point with $P=7.983W$

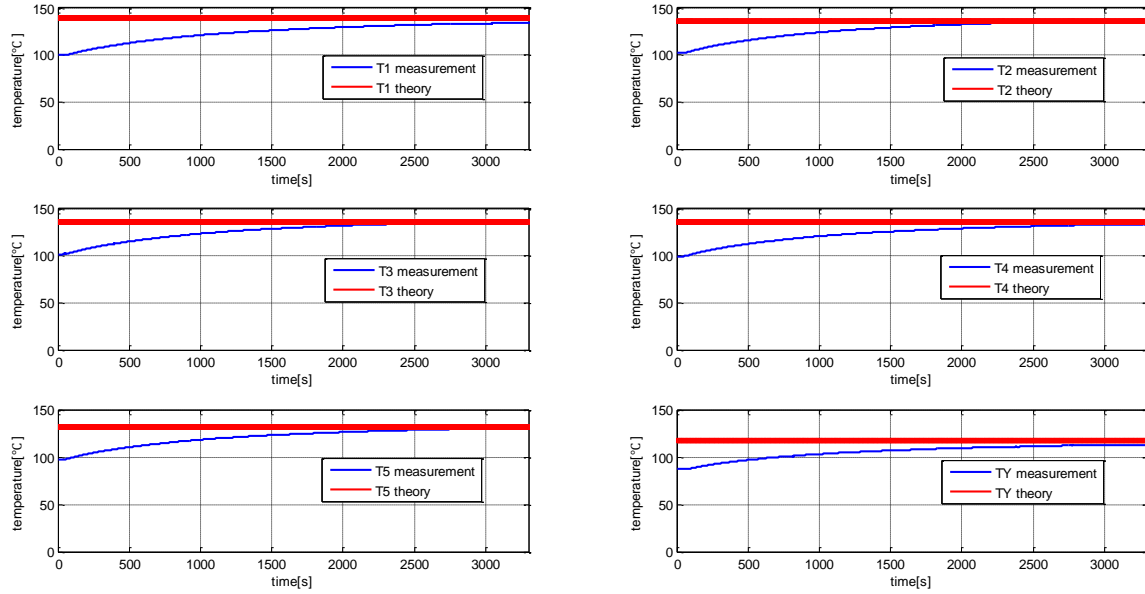


Fig. 5.17: Temperature difference of each point with $P=12.062W$

Table 5.7 shows the percentage of error between the measured and theoretical values in different conducted powers. The biggest absolute error is about 4% which proves that the thermal resistances measured in the first phase are correct.

Table 5.7: Error percentage of each temperature

No.	P(W)	T1(°C)	T2(°C)	T3(°C)	T4(°C)	T5(°C)	TY(°C)
1	2.815	-0.4%	2.3%	2.3%	1.8%	1.9%	1.5%
2	7.983	-2.5%	1.3%	1.3%	-0.8%	0.2%	-1.4%
3	12.062	-3.8%	0.3%	0.4%	-1.7%	-0.9%	-4.0%

5.2.3 Simulation in PLECS

A good way to validate the measured results is to simulate in program. In real life, it is difficult to test all the parameters of every new product. So it will be easier and more economical to effectuate some simulations in software. In this part, a brief introduction of the software PLECS (Piecewise Linear Electrical Circuit Simulation) and how to organize the program will be given.

PLECS is a Simulink toolbox developed by Plexim for system-level simulation of electrical circuits [19]. It is one of the best design platforms for power electronics systems because of its

high-speed simulation. In this part, both the electrical and thermal circuits are visualized in Fig. 5.18 where the module Heat Sink acts as their interface.

For the electrical part (dash-line-rectangle), five variable resistors are used to represent the five layers of windings of the transformer. As it was mentioned in (2.9), copper wire has a positive temperature coefficient (PTC) which should be taken into account during the calculation of its actual resistance. So a subsystem shown in Fig. 5.19 can be designed to control the change of the variable resistor. The input of the subsystem comes from the temperature of each thermal resistance. Thus each variable resistor and each thermal resistance constitute a closed loop feedback system. See Fig. 5.20. When the thermal resistance of each layer is determined, the temperature will be decided by the input voltage uniquely.

Fig. 5.21 shows the input power has a decreasing tendency because of the increasing resistance.

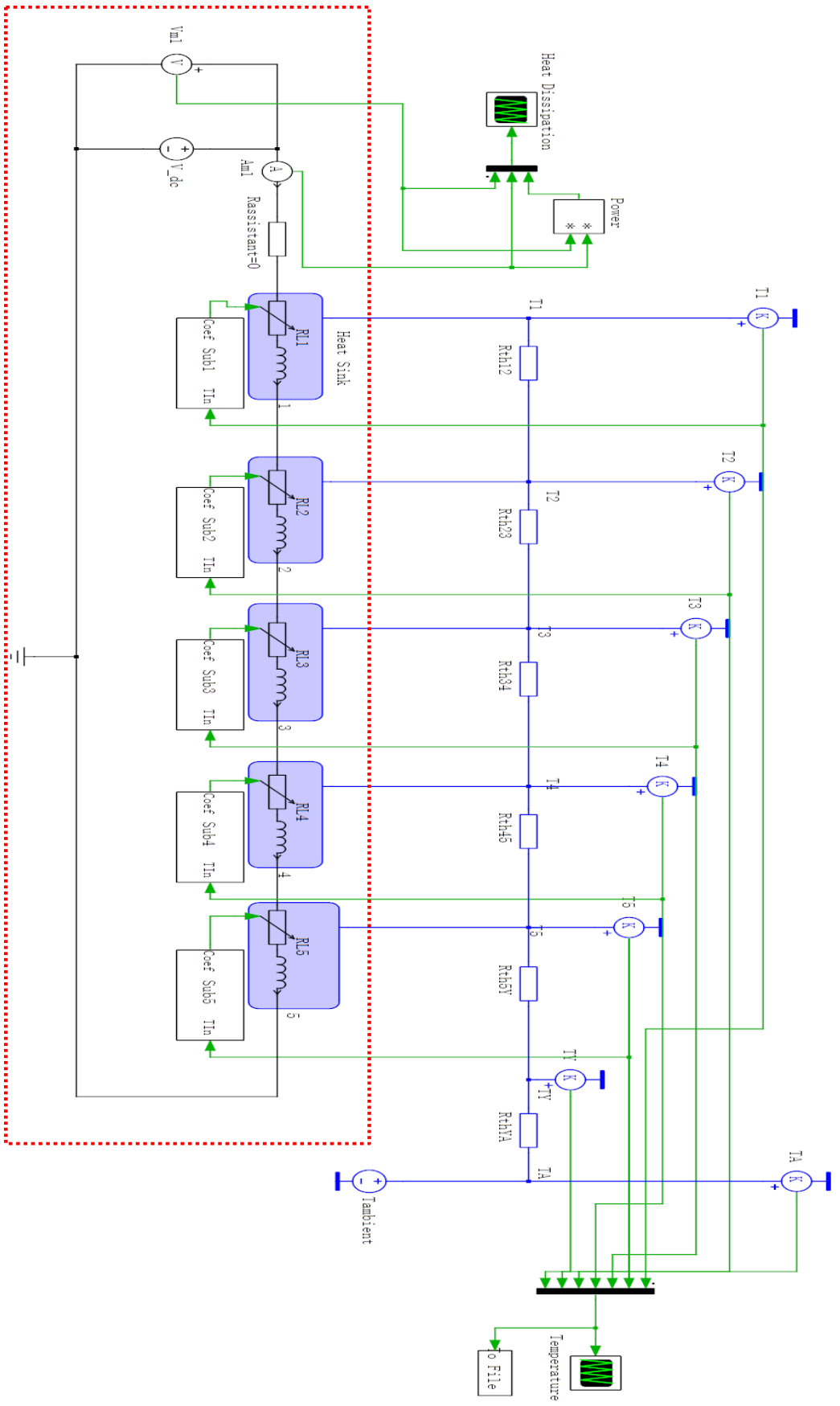


Fig. 5.18: Thermal and electrical model

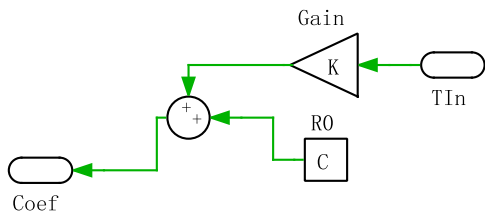


Fig. 5.19: The subsystem for $R_T = R_0(1 + \Delta T\alpha)$

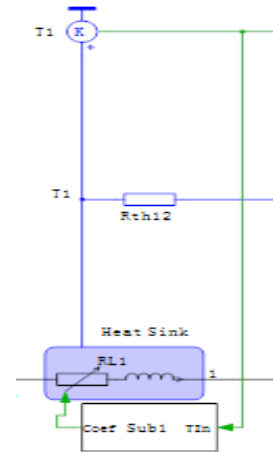


Fig. 5.20: The closed loop feedback

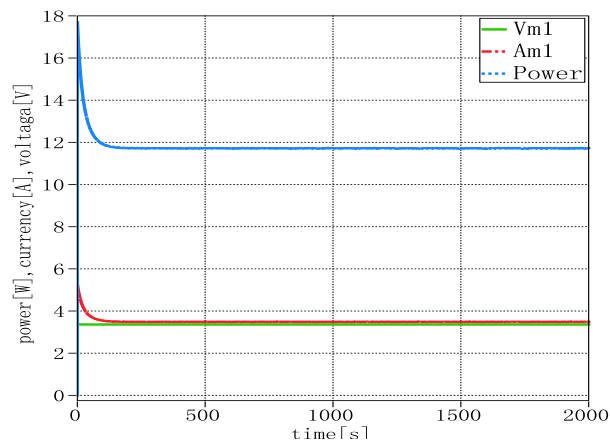


Fig. 5.21: The variation of the resistance

Fig. 5.22 to Fig. 5.24 illustrate the simulation results at the same power dissipation of the test in Section 5.2.2.

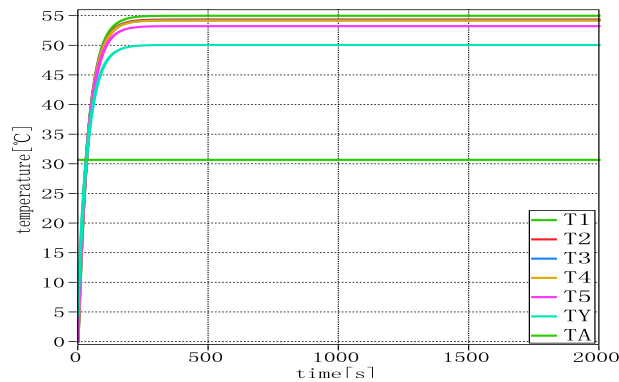


Fig. 5.22: Simulation results with $P=2.815W$

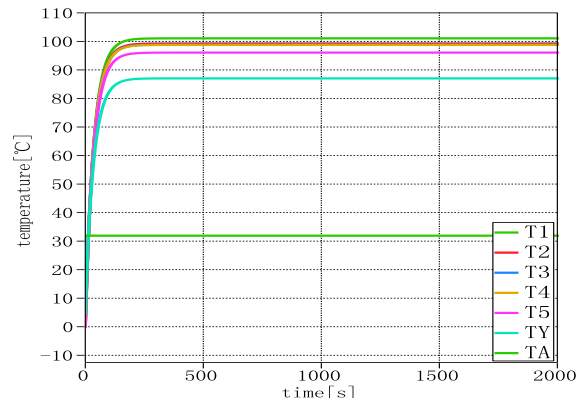


Fig. 5.23: Simulation results with $P=7.983W$

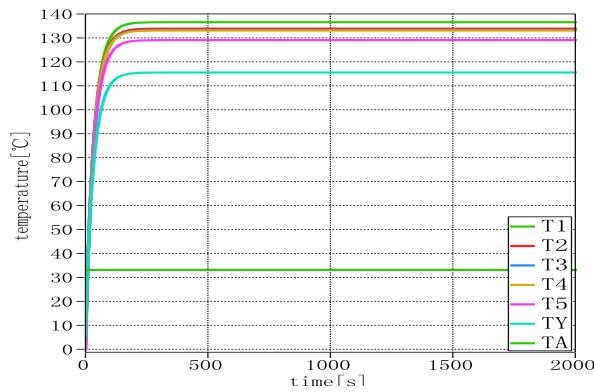


Fig. 5.24: Simulation results with $P=12.026W$

Table 5.8 shows the temperature of each point simulated in PLECS. Table 5.9 is the comparison between the temperature measured in the experiment and produced in PLECS. We can see that the biggest absolute error percentage is 3.2% which means the simulation is correct.

Table 5.8: Simulation results

No.	P(W)	T1(°C)	T2(°C)	T3(°C)	T4(°C)	T5(°C)	TY(°C)
1	2.815	54.98	54.35	54.21	54.17	53.23	50.05
2	7.983	101.07	99.28	98.88	98.77	96.08	87.04
3	12.062	136.56	133.87	133.27	133.10	129.07	115.55

Table 5.9: Error between the simulated and measured results

No.	P(W)	T1(°C)	T2(°C)	T3(°C)	T4(°C)	T5(°C)	TY(°C)
1	2.815	0.5%	2.9%	3.2%	2.8%	2.8%	2.3%
2	7.983	-1.3%	2.6%	2.5%	0.4%	1.4%	-0.2%
3	12.062	-1.7%	2.4%	2.5%	0.4%	1.2%	-2.0%

5.2.4 Conclusion for test 1

In test 1, the thermal resistances were derived from the measured temperatures and they were used to predict the temperature in different power dissipations. Then the other measurement and simulation were effectuated successively and their results proved the thermal resistances were correctly calculated. Nevertheless there exists a large inconvenience because in the industrial domain, it is impossible to place the sensors in each product to measure their temperatures. So we need to be able to calculate the thermal resistance basing on the material used in the transformer and the theoretical results should match the measured ones. The largest significance of that case lies on the general applicability to all the similar products as long as the module's parameters are established. That is the reason why test 2 is carried out.

5.3 Test 2- With interlayer thermal insulation

In this section, at first a theoretical calculation of the thermal resistance will be made. Then on the basis of the theory, a new model will be built to examine if the theoretical and measured values match each other properly. From test 1, we can notice that the thermal resistance of each layer was so small because of the high heat conductivity of copper wire (about 380 W/m.k), which can be beyond the resolving ability of the PT sensor. So some interlayer thermal insulation tapes with known thermal conductivity will be added. Fig. 4.5 to Fig. 4.7 showed the manufacture sketch for test 2.

5.3.1 Heating source

In the first phase of test 1, an external resistor put inside the coil former was used to act as the heating source. But it is not so perfect because the resistor can't be placed manually exactly in the middle of the coil former. In most cases, the resistor inclines to one side of the coil former. According to the data sheet provided by manufacturer, the coil former is made of PET (Polyethylene Terephthalate) which has low heat conductivity (about 0.15W/m.k), so the temperature of the whole coil former is not homogeneous. To some extent, ΔT depends on the position where the PT sensor is located. There is why some negative thermal resistances occurred in test 1. Thus in test 2, an extra layer of winding that has not any electrical connection to the other ones is made to act as the heating source.

5.3.2 Coil former test

The characteristic parameter of the coil former has been visualized in Fig. 4.2. Even though its heat conductivity is not provided, we can apply the one of PET for the calculation. Fig. 5.25 (a) shows the construction of the coil former test. The layer of copper wire is used to get a homogeneous heating environment. Fig. 5.25 (b) and (c) show the structure and the heat flow direction respectively.

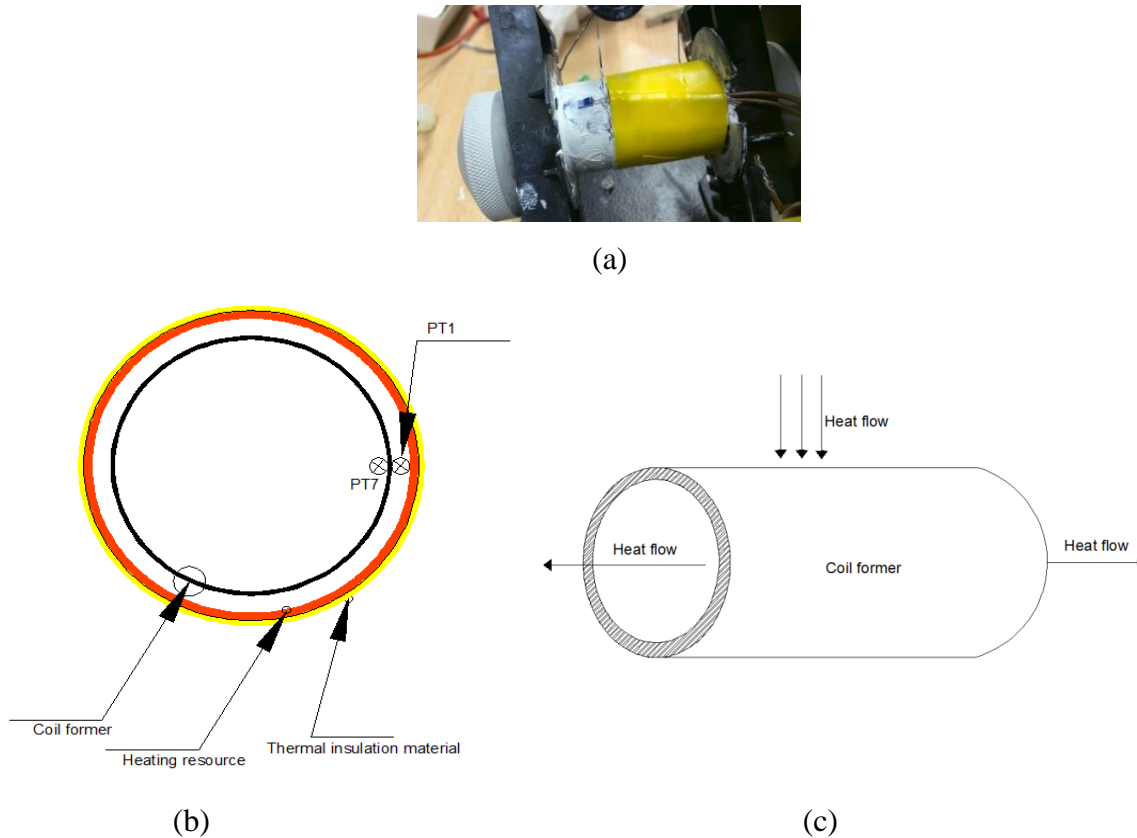


Fig. 5.25: (a) Construction of the coil former test (b) Structure form top view (c) Heat flow direction from side view

5.3.2.1 Theoretical calculation and measured results

For hollow cylinder, the calculation of thermal resistance can be presented as

$$R_{th} = \frac{\ln \frac{r_2}{r_1}}{2\pi kl} \quad (5.24)$$

where, r_1 is inside radius, r_2 is outside radius, k is heat conductivity and l is length [20].

Fig. 5.25 shows the precise dimensions and the heat flow direction of the coil former test.

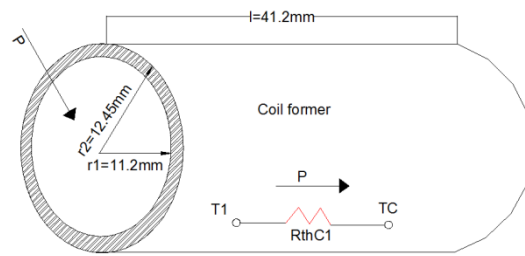


Fig. 5.26: Coil former dimensions for test

According to the property of the material, the theoretical thermal resistance can be presented in Table 5.10 by using (5.24).

Table 5.10: Theoretical thermal resistance of the coil former

Item	Theoretical value				
	r2(m)	r1(m)	l(m)	K(w/m.k)	R_{th} (°C/w)
Coil former	0.01245	0.0112	0.0412	0.15	2.725

Then the extra winding is conducted with different DC powers to measure the real thermal resistance of the coil former.

Figs 5.27 to Fig. 5.29 show the difference between the theoretical and measured values.

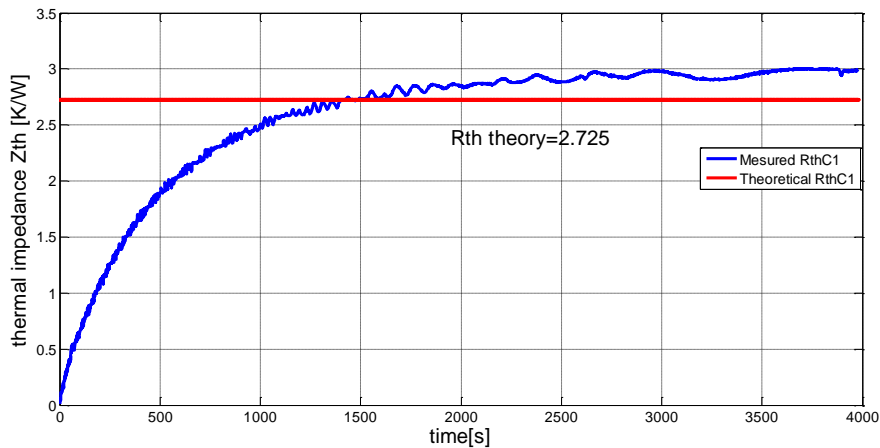


Fig. 5.27: Thermal impedance difference with $P=2.159W$

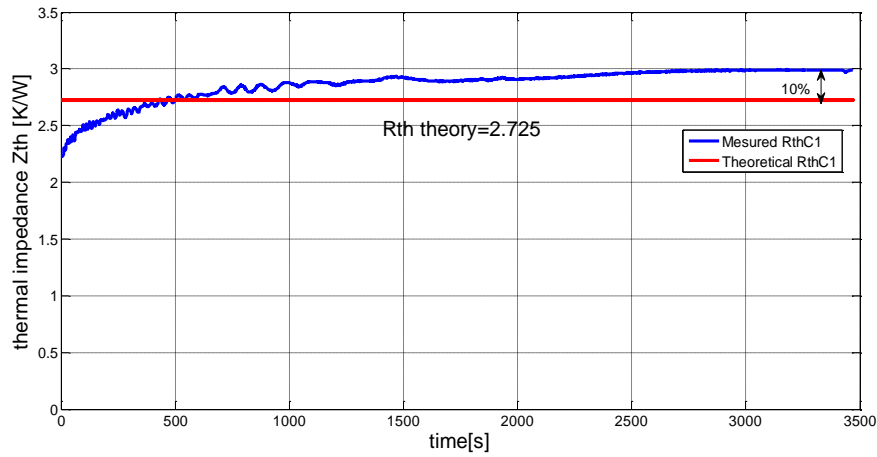


Fig. 5.28: Thermal impedance difference with $P=2.898\text{ W}$

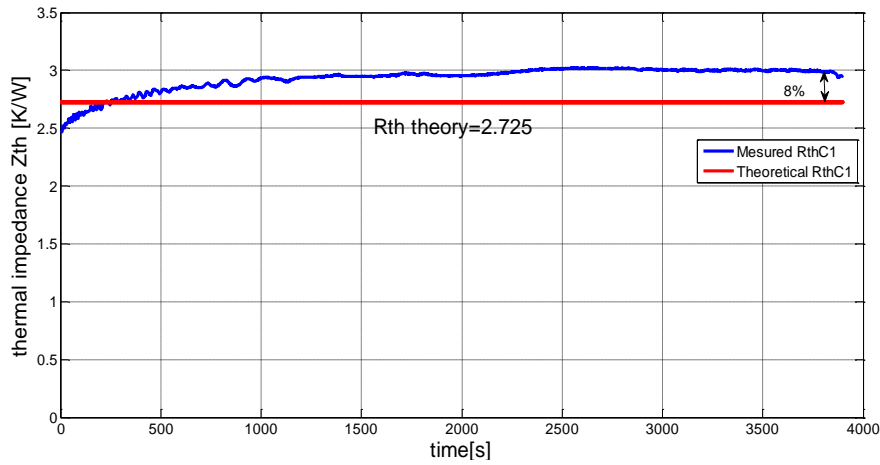


Fig. 5.29: Thermal impedance difference with $P=3.524\text{ W}$

From Table 5.11, we can see that the average error is about 9% and the measured values are always larger than the theoretical ones. This is probably caused by the thermal conductivity of the coil former material for the reason that it is made by impure PET.

Table 5.11: Comparison between theoretical and measured values

NO.	measurement			theory	Error
	$P(w)$	$\Delta T(^{\circ}C)$	$R_{th}(^{\circ}C/w)$	$R_{th}(^{\circ}C/w)$	-
1	1.440	4.262	2.959	2.725	9%
2	2.159	6.463	2.993		10%
3	2.898	8.657	2.987		10%
4	3.524	10.404	2.952		8%
Average	-	-	2.973		9%

The entire test for the coil former should be effectuated under the condition that the coil former is in the erect position which is visualized as Fig. 5.30 (a). If it is placed horizontally as Fig. 5.30 (b), it can bring a larger error. See Table 5.12.



Fig. 5.30: (a) Upright position, (b) horizontal position

Table 5.12: Measured result in horizontal position

NO.	$P(w)$	measured		theoretical	error
		$\Delta T(^{\circ}C)$	$Rth(^{\circ}C/w)$	$Rth(^{\circ}C/w)$	-
1	1.402	6.127	4.369	2.725	60%

Fig. 5.31 shows the temperature difference between the top side and bottom side of the coil former when it was placed horizontally. This is because of the heat convection causes the hot-air accumulates at the top side.

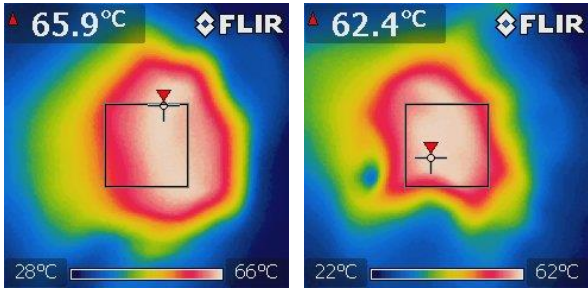


Fig. 5.31: (a) Top side temperature, (b) bottom side temperature

5.3.3 Core test

In this part, the EPCOS ferrite core ETD59 is used to test. The dimensions of the core are visualized in Fig. 4.3. In order to fill in the air gap between the coil former and the core, three layers of insulation tape with heat conductivity (0.9w/m.k) are added which is shown in Fig. 5.32.



Fig. 5.32: Test for the core ETD59

When the core is plugged into the coil former, the outside of the core is covered with thermal insulation material except for its top side middle. See Fig. 5.33.

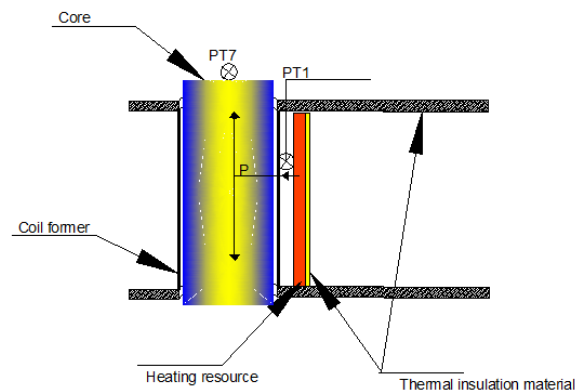


Fig. 5.33: Sketch for the core test

This measurement bases on the test of the coil former, so the equivalent thermal network is presented as Fig. 5.34.

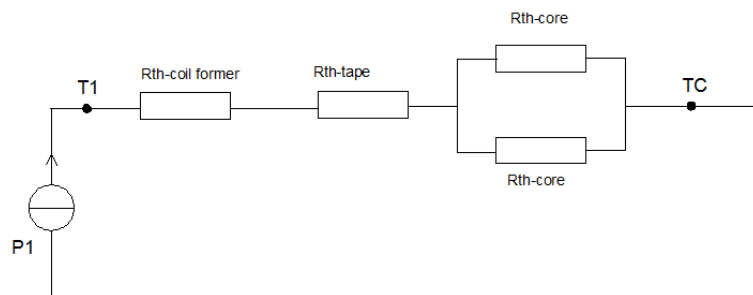


Fig. 5.34: Thermal network of the core and coil former

where $R_{th-coil\ formr}$ is the thermal resistance of the coil former, $R_{th-tape}$ is the thermal resistance of the insulation tape, $R_{th-core}$ is the thermal resistance of the ferrite core, P_1 is the heating source, T_1 is the temperature on the surface of the coil former, T_c is the temperature on the surface of the ferrite core.

According to the parameter provided by manufacturer, the thermal resistance of ETD59 core is $4^{\circ}\text{C}/\text{w}$, but in this test, the core is regarded as two halves which are connected parallely, so the equivalent value is $1^{\circ}\text{C}/\text{w}$ in this thermal network.

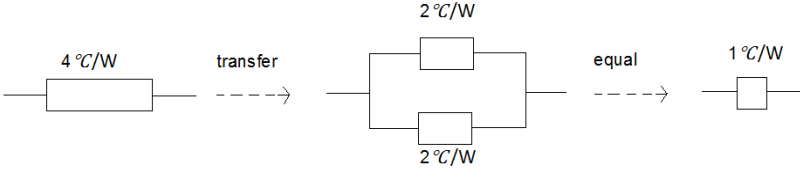


Fig. 5.35: Thermal network the core and coil former

5.3.3.1 Theoretical calculation and measured results

The thermal resistance of the coil former is taken from the average measured value in the previous test, so the theoretical thermal resistance of the test is presented in Table 5.13.

Table 5.13: Theoretical value

Item	coil former	insulation tape	ferrite core	Total
$R_{th} (^{\circ}\text{C}/\text{w})$	2.973	0.052061	1.0	4.025

The thermal impedance differences are visualized in Fig. 5.36 to Fig. 5.38 with different power dissipations.

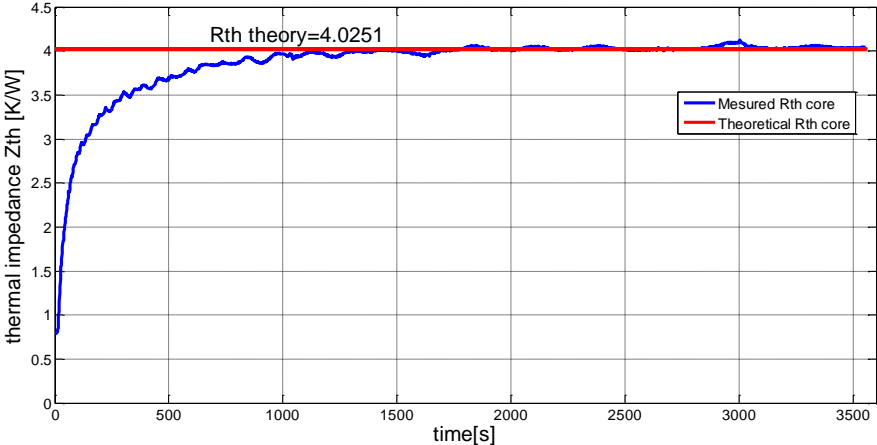


Fig. 5.36: Thermal impedance difference with $P=2.016\text{W}$

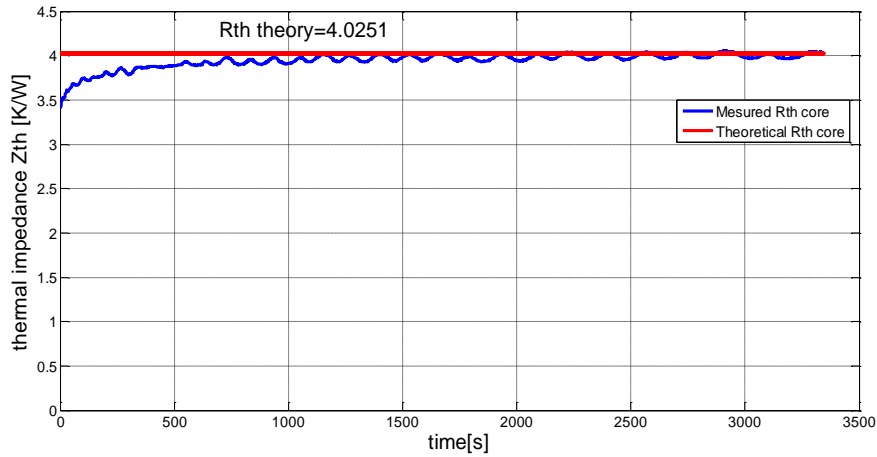


Fig. 5.37: Thermal impedance difference with $P=2.531W$

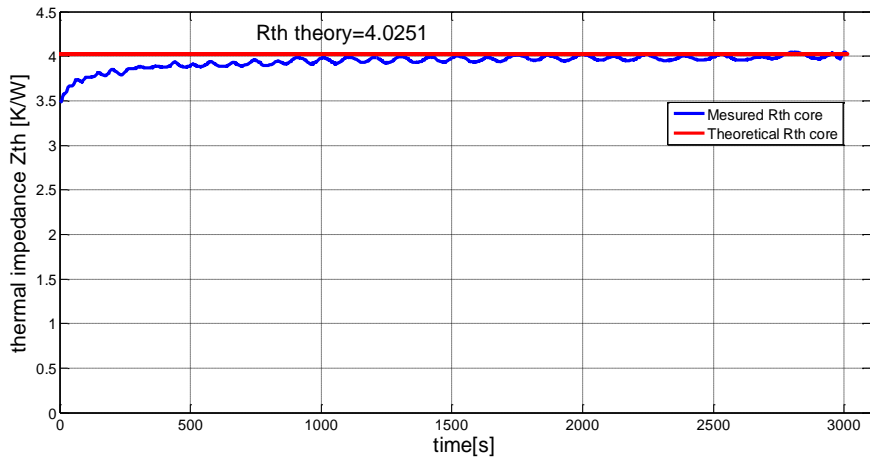


Fig. 5.38: Thermal impedance difference with $P=3.043W$

Table 5.14 shows the error between the theoretical and measured values. The biggest absolute error is about 0.4% which proves that the theoretical and measured values match each other perfectly.

Table 5.14: Comparison between the theoretical and measured values

measurement				theory	Error
NO.	$P(w)$	$\Delta T(^{\circ}C)$	$Rth(^{\circ}C/w)$	$Rth(^{\circ}C/w)$	-
1	2.016	8.149	4.042	4.025	-0.4%
2	2.531	10.171	4.019		0.2%
3	3.043	12.263	4.030		-0.1%

5.3.4 Windings test

In this test, an extra layer of copper wire is added besides the five layers windings to act as the heating source. The heat flow dissipates through the five layer windings and the core. Once the temperature difference between each layer is measured, the thermal resistance can be decided by (2.12). Fig. 5.39 shows the experiment model.

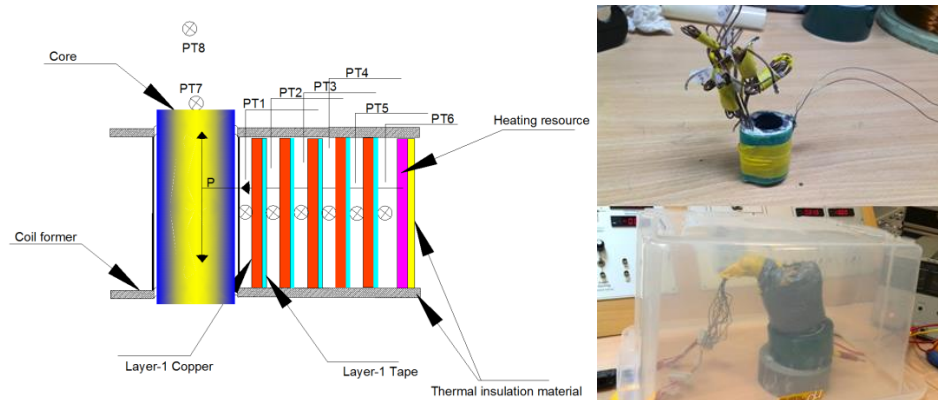


Fig. 5.39: Windings test

5.3.4.1 Theoretical calculation

R_{thCA} test:

For the calculation of R_{thCA} , it is much more complex as it involves energy dissipation between a solid surface and the air. Three thermal transport mechanisms occur at the same time. But because of the low heat conductivity of the air ($k=0.032W/m.k$), for simple reason, the heat transported by conduction can be negligible.

According to Newton's law of cooling, the energy transported by convection can be derived as

$$q_{conv} = hA(T_1 - T_A) \quad (5.25)$$

where h is convection heat-transfer coefficient, A is area, T_1 is the temperature of the core, T_A is the ambient temperature.

In this test, the model is put into a chamber, so the convection can be considered as natural convection. It concerns three dimensionless parameters: Nusselt number (Nu), Prandtl number (Pr) and Grashof number (Gr). The relationship between h and Nu can be presented as

$$Nu = hL/k \quad (5.26)$$

where L is a characteristic dimension of the solid object, k is the thermal conductivity of the fluid.

If Nu is decided, h can be easily deduced.

Generally, the three dimensionless parameters follow the relationship as

$$Nu = c(G_r P_r)^n \quad (5.27)$$

where c is the thermal property of the air, n is decided by the product of $G_r P_r$: if $G_r P_r < 10^8$, the convection is laminar flow, $n=0.33$; if $G_r P_r > 10^8$, $n=0.25$ for turbulent flow.

In most cases, we can judge the state of the flow by using the product of $L^3 \Delta T$, if $L^3 \Delta T > 1$, it can be considered as turbulent flow, otherwise it is laminar flow. In this test, the temperature difference is small enough, so the convection is laminar flow. Then an empirical equation can be used to calculate h [21].

$$h = 1.42 \left(\frac{\Delta T}{L} \right)^{0.25} \quad (5.28)$$

For the radiation, the transferred energy can be presented by Stefan-Boltzmann law

$$q_{rad} = \varepsilon \sigma A (T_1^4 - T_A^4) \quad (5.29)$$

where ε is emissivity of the core, σ is Stefan-Boltzmann constant, $\sigma = 5.669 \times 10^{-8} \text{ W.m}^{-2} \text{ K}^{-4}$, T_1 and T_A are thermodynamic temperature in Kelvin.

So the total heat dissipation can be presented as

$$q_{total} = q_{conv} + q_{rad} \quad (5.30)$$

$$q_{total} = hA\Delta T + \varepsilon \sigma A (T_1^4 - T_A^4) \quad (5.31)$$

The total thermal resistance can be written as

$$R_{th} = \frac{\Delta T}{q_{total}} = \frac{\Delta T}{hA\Delta T + \varepsilon \sigma A (T_1^4 - T_A^4)} \quad (5.32)$$

Table 5.15 shows the difference between the theoretical and measured values. This error may be caused by the imperfect thermal insulation which means that not all the energies dissipate through the core.

Table 5.15: Comparison between the theoretical and measured values

NO	$A(m^2)$	theoretical				measured	error
		$h(W/m^2 \cdot ^\circ C)$	$\Delta T(^{\circ}C)$	ε	$R_{th}(^{\circ}C/w)$	$R_{th}(^{\circ}C/w)$	-
1	0.00264	8.4	27.01	0.9	25.413	27.682	-8%
2	0.00264	9.3	41.04	0.9	23.254	27.705	-16%

Interlayer thermal resistance calculation:

For the calculation of the thermal resistance of each layer, (5.24) can be applied. The diameter of the copper wire used in this test is 0.40mm and the thickness of the tape is 80um. Table 5.16 shows the theoretical values of each layer.

Table 5.16: Theoretical calculation

	material	$K(w/m.k)$	$D2(2*r2)$	$D1(2*r1)$	$l(m)$	$R_{th}(^{\circ}C/w)$
R_{th12}	copper	377	0.0257	0.0249	0.0412	0.00032
	Tape	0.15	0.02666	0.0257	0.0412	0.94446
	total					0.94478
R_{th23}	copper	377	0.02746	0.02666	0.0412	0.00030
	Tape	0.15	0.02842	0.02746	0.0412	0.88495
	total					0.88525
R_{th34}	copper	377	0.02922	0.02842	0.0412	0.00028
	Tape	0.15	0.03018	0.02922	0.0412	0.83250
	total					0.83278
R_{th45}	copper	377	0.03098	0.03018	0.0412	0.00027
	Tape	0.15	0.03178	0.03098	0.0412	0.65659
	total					0.65685
R_{th5Y}	copper	377	0.03258	0.03178	0.0412	0.00025
	Tape	0.15	0.03338	0.03258	0.0412	0.62473
	total					0.62498

where D1 and D2 are diameters for each layer.

After the measurement, the results and the comparison are listed at Table 5.17.

Table 5.17: Comparison and error percentage

No.	$P(w)$	measurement			theory	error
		Item	$\Delta T(^{\circ}C)$	$R_{th}(^{\circ}C/w)$	$R_{th}(^{\circ}C/w)$	-
1	1.4055	R_{th12}	1.308	0.930	0.944	-1%
		R_{th23}	1.319	0.938	0.885	6%
		R_{th34}	1.205	0.857	0.833	3%
		R_{th45}	0.893	0.635	0.657	-3%
		R_{th5Y}	0.905	0.644	0.625	3%
2	1.9511	R_{th12}	1.869	0.958	0.944	-1%
		R_{th23}	1.698	0.870	0.885	2%
		R_{th34}	1.536	0.787	0.833	6%
		R_{th45}	1.220	0.625	0.657	5%
		R_{th5Y}	1.238	0.635	0.625	-2%
3	2.9625	R_{th12}	2.895	0.977	0.944	-3%
		R_{th23}	2.528	0.853	0.885	4%
		R_{th34}	2.323	0.784	0.833	6%
		R_{th45}	1.798	0.607	0.657	8%
		R_{th5Y}	1.873	0.632	0.625	-1%

For a clearer view, we can make the comparison based on the average values at Table 5.18.

Table 5.18: Comparison based on average values

	measurement	theory	error
Item	$R_{th}(^{\circ}C/w)$	$R_{th}(^{\circ}C/w)$	-
R_{th12}	0.955	0.944	1%
R_{th23}	0.887	0.885	0.3%
R_{th34}	0.810	0.833	-3%
R_{th45}	0.622	0.657	-5%
R_{th5Y}	0.637	0.625	2%

We can see that the largest absolute error is 5% which can be accepted in the test.

Fig. 5.40 to Fig. 5.42 show the difference between the theoretical and measured thermal impedance of each layer in different power.

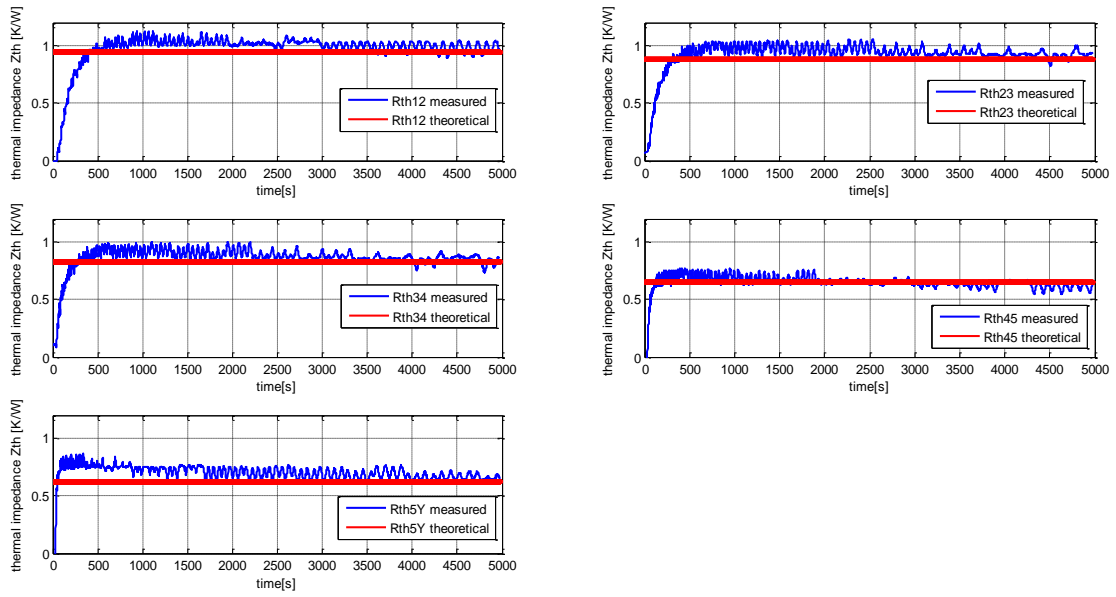


Fig. 5.40: Thermal impedance difference with $P=1.406W$

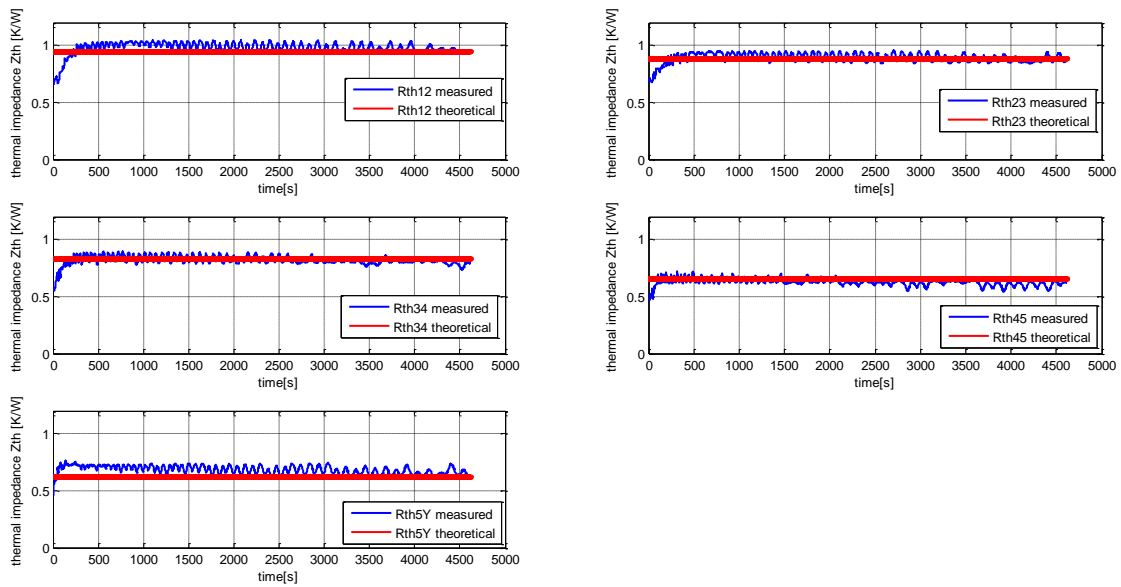


Fig. 5.41: Thermal impedance difference with $P=1.951W$

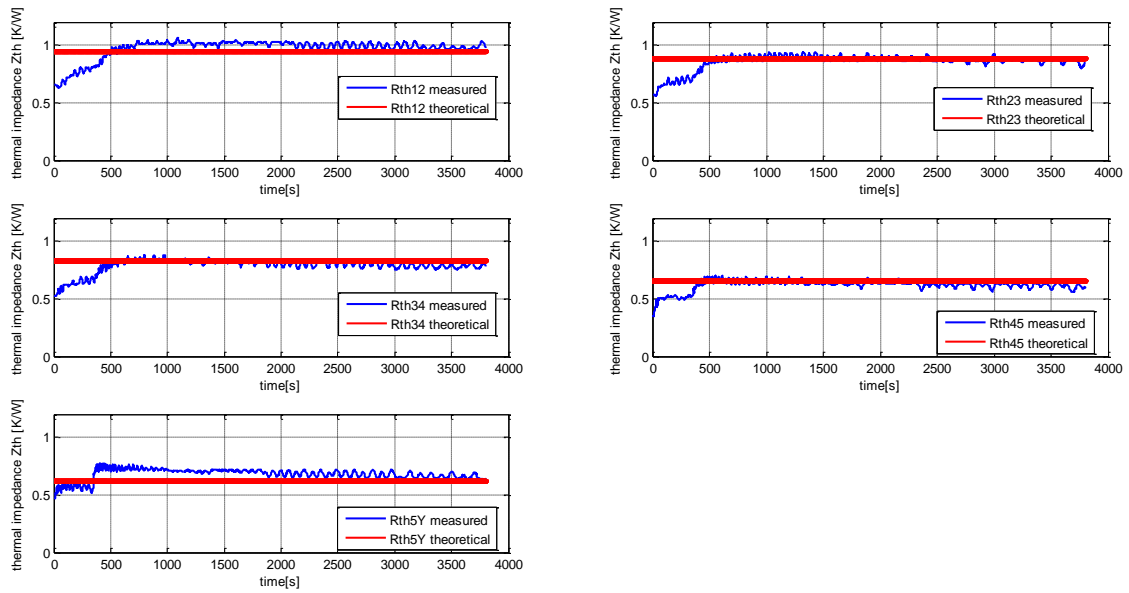


Fig. 5.42: Thermal impedance difference with $P=2.963W$

R_{thYA} test:

In this test, the heat transportation direction is inverse compare to the winding test. So the first layer copper wire is used to be the heating source. Fig. 5.43 illustrates the precise form.

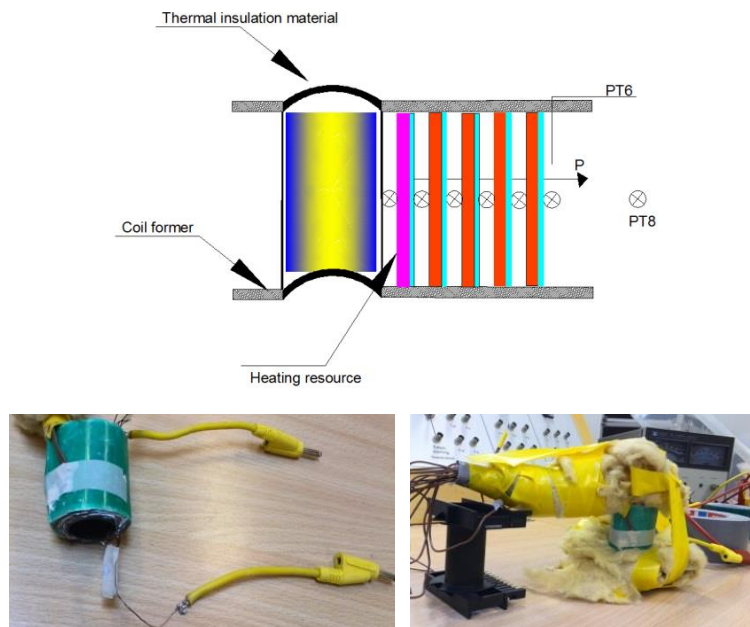


Fig. 5.43: R_{thYA} test

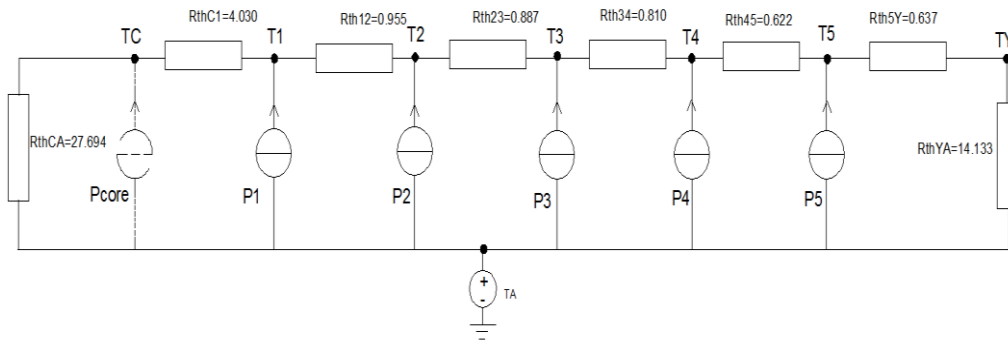
By applying the same principles at 5.3.1, the theoretical and measured values is presented in Table 5.19

Table 5.19: Comparison between the theoretical and measured values

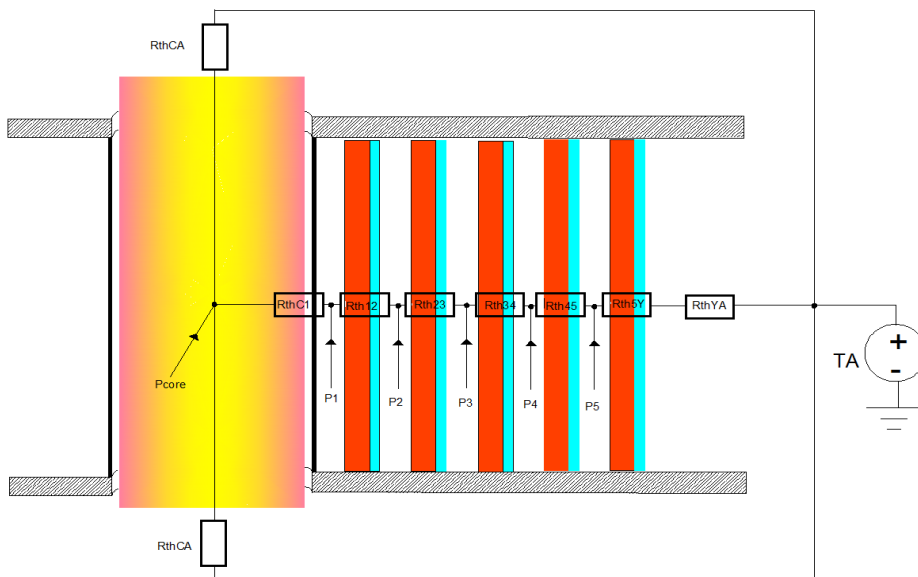
N0	theoretical						measured	error
	$A(m^2)$	$h(W/m^2 \cdot ^\circ C)$	$\Delta T(^{\circ}C)$	ε	$\sigma(W/m^2 K^4)$	$R_{th}(^{\circ}C/w)$	$R_{th}(^{\circ}C/w)$	-
1	0.00432	7.4	24.02	0.9	$5.67e-8$	16.830	14.489	-14%
2	0.00432	8.0	32.87	0.9	$5.67e-8$	15.817	14.342	-9%
3	0.00432	8.4	40.58	0.9	$5.67e-8$	15.111	13.567	-10%

5.3.5 The whole thermal network

After all the thermal resistances have been measured and compared, the complete thermal network can be illustrated as Fig. 5.44. This network applies to both AC and DC. For the usage in AC, firstly, the core losses should be calculated by taking the eddy loss and the hysteresis loss into account.



(a)



(b)

Fig. 5.44: The complete thermal network for a five-layer transformer

Chapter 6

6. Conclusion and future work

6.1 Conclusion

The main objective of this project is to establish a thermal model of a transformer based on measurement data. The model should apply to any similar transformer and has not limit in the number of layer. Under this condition, a series of tests have been carried out.

Chapter 3 mainly described the temperature measurement system which was needed during the whole project. This system was the combination of hardware and software. For the hardware, a brief description for PCB was made. As to the software, it consisted of LabVIEW and Matlab.

Then two main tests were implemented. Test 1 aimed at the prediction of the temperature based on the measured thermal resistance. This prediction was compared to the measured values and they matched each other perfectly. Besides, a simulation using PLECS was also effectuated to verify this thermal modelling. The important significance of Test 1 lied on the precise prediction of the temperature according to the conducted current. However, this thermal model was suitable uniquely to the transformer made in Test 1.

That was the reason why Test 2 was done. It focused on the theoretical calculation of the thermal resistance on the basis of the material used in the transformer. These values practically conformed to the measured ones. The advantage of the thermal model in Test 2 was that it was applicable for any similar transformer at any number of layers.

6.2 Future work

For the next step of this work, some points need to be improved.

Firstly, the key factors which decide the interlayer thermal resistances should be determinated. As it was mentioned before, the copper wires were greased to reduce the influence of the contact thermal resistance as well as the porosities. In the industrial product, this phenomenon is very rare.

Secondly, a better method FEM should be carried out to analyze the thermal situation. The best challenge of that is the modelling of the 3-Dimensions coordinate system which can take some time.

Then the final model should be conducted with AC to verify its response.

Lastly, the capacitance of each layer can be derived based on the curves. According to a RC circuit, the time constant can be described as $\tau = RC$, τ presents the time it takes for the system response to reach 63.2% of its final value. Since R is already know, τ can be read from the curve, and then C can be calculated. If so, a totally complete thermal network will be constructed and the transient response can be displayed.

References

- [1] "Transformer," web page. Available: <http://en.wikipedia.org/wiki/Transformer>
- [2] Olivier MALOBERTI, "Material of Electrical Energy," ESIEE-Amiens, appendix-1, 2013
- [3] "Convection, conduction and radiation," Web page. Available:
<http://www.mansfieldct.org/Schools/MMS/staff/hand/convcondrad.htm>
- [4] "Thermal analysis of semiconductor systems," Web page. Available:
http://cache.freescale.com/files/analog/doc/white_paper/BasicThermalWP.pdf pp.6
- [5] JI Hai-ning, LAN Zhong-wen, ZHANG Huai-Wu, Zhang Yue, "Thermal Simulation of Switching Mode Power Supply Transformer With ANSYS," Journal of Magnetic Materials and Devices, pp.1, 2006
- [6] "Thermometer," web page. Available: <http://baike.baidu.com/view/41148.htm>
- [7] "Select a sensor," web page. Minco. Available:
<http://www.minco.com/Sensors-and-Instruments/Support-and-Tools/Select-a-Sensor>
- [8] "Transformer," web page. Available: <http://baike.baidu.com/view/30130.htm>
- [9] "Resistance thermometer," web page. Available:
http://en.wikipedia.org/wiki/Resistance_thermometer#cite_note-2
- [10] P. R. N. Childs, "Practical temperature measurement," Oxford, Boston: Butterworth-Heinemann, pp.149, 2001
- [11] "Measuring temperature with rtds-a tutorial," National instruments, 1996. Available:
<http://newton.ex.ac.uk/teaching/CDHW/Sensors/an046.pdf>
- [12] "Ina122 instrumentation amplifier data sheet," Texas instrument, 2013. Available:
<http://www.ti.com/lit/ds/symlink/ina122.pdf>
- [13] Kang Hua guang, "Technology of analog signal," pp.415-417, 2005
- [14] "Protues", web page. Available:
<http://baike.baidu.com/view/1639293.htm?fr=wordsearch>
- [15] "Calibration", web page. Available: <http://en.wikipedia.org/wiki/Calibration>
- [16] "Polyt é r phthalate d' é thyl è ne ", web page. Available:
http://fr.wikipedia.org/wiki/Polyt_é_r_phthalate_d'_é_thyl_è_ne
- [17][20][21] J.P. Holman, "Heat Transfer," pp.59, pp.55, pp.346, 2008
- [18] Qiu Guanyuan, "Circuit theory," pp.60-64, 2006
- [19] "Electrical engineering software," Plexim, 2013, web page. Available:
<http://www.plexim.com/>

Appendix A

Component data sheet



**Single Supply, *MicroPower*
INSTRUMENTATION AMPLIFIER**

FEATURES

- LOW QUIESCENT CURRENT: 60µA
- WIDE POWER SUPPLY RANGE
Single Supply: 2.2V to 36V
Dual Supply: -0.9/+1.3V to ±18V
- COMMON-MODE RANGE TO (V-) -0.1V
- RAIL-TO-RAIL OUTPUT SWING
- LOW OFFSET VOLTAGE: 250µV max
- LOW OFFSET DRIFT: 3µV/°C max
- LOW NOISE: 60nV/√Hz
- LOW INPUT BIAS CURRENT: 25nA max
- 8-PIN DIP AND SO-8 SURFACE-MOUNT

APPLICATIONS

- PORTABLE, BATTERY OPERATED SYSTEMS
- INDUSTRIAL SENSOR AMPLIFIER:
Bridge, RTD, Thermocouple
- PHYSIOLOGICAL AMPLIFIER:
ECG, EEG, EMG
- MULTI-CHANNEL DATA ACQUISITION

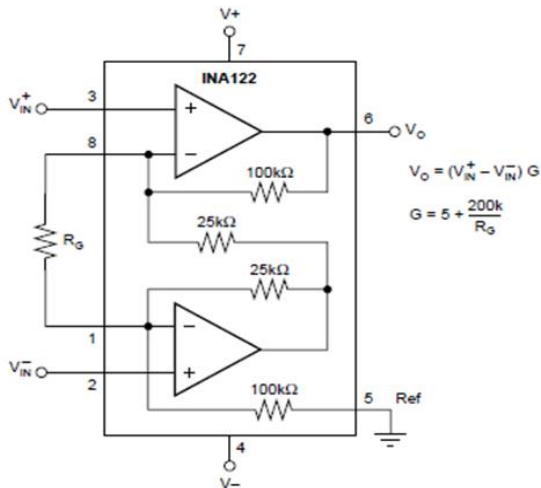
DESCRIPTION

The INA122 is a precision instrumentation amplifier for accurate, low noise differential signal acquisition. Its two-op-amp design provides excellent performance with very low quiescent current, and is ideal for portable instrumentation and data acquisition systems.

The INA122 can be operated with single power supplies from 2.2V to 36V and quiescent current is a mere 60µA. It can also be operated from dual supplies. By utilizing an input level-shift network, input common-mode range extends to 0.1V below negative rail (single supply ground).

A single external resistor sets gain from 5V/V to 1000V/V. Laser trimming provides very low offset voltage (250µV max), offset voltage drift (3µV/°C max) and excellent common-mode rejection.

Package options include 8-pin plastic DIP and SO-8 surface-mount packages. Both are specified for the -40°C to +85°C extended industrial temperature range.



$$V_O = (V_{IN+} - V_{IN-}) G$$

$$G = 5 + \frac{200k}{R_G}$$

Fig. A.1: INA122 data sheet

SPECIFICATIONS

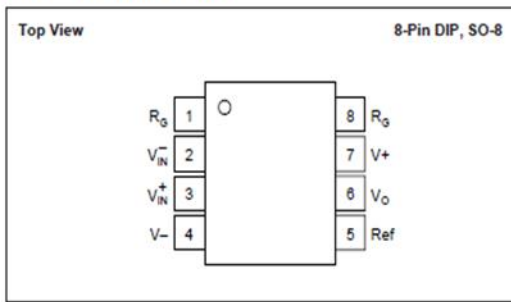
At $T_A = +25^\circ\text{C}$, $V_O = +5\text{V}$, $R_L = 20\text{k}\Omega$ connected to $V_O/2$, unless otherwise noted.

PARAMETER	CONDITIONS	INA122P, U			INA122PA, UA			UNITS	
		MIN	TYP	MAX	MIN	TYP	MAX		
INPUT									
Offset Voltage, RTI	$V_O = +2.2\text{V to } +36\text{V}$		± 100	± 250		± 150	± 500	μV	
vs Temperature			± 1	± 3		*	± 5	$\mu\text{V}/^\circ\text{C}$	
vs Power Supply (PSRR)				10	30		*	100	$\mu\text{V/V}$
Input Impedance				$10^{10} \parallel 3$			*		$\Omega \parallel \text{pF}$
Safe Input Voltage	$R_G = 0$	$(V^-) - 0.3$		$(V^+) + 0.3$	*		*	V	
	$R_G = 10\text{k}\Omega$	$(V^-) - 40$		$(V^+) + 40$	*		*	V	
Common-Mode Voltage Range		0		3.4	*		*	V	
Common-Mode Rejection	$V_{CM} = 0\text{V to } 3.4\text{V}$	83	96		76	90		dB	
INPUT BIAS CURRENT									
vs Temperature			-10	-25		*	-50	nA	
Offset Current			± 40			*		$\text{pA}/^\circ\text{C}$	
vs Temperature			± 1	± 2		*	± 5	nA	
			± 40			*		$\text{pA}/^\circ\text{C}$	
GAIN			$G = 5 \text{ to } 10\text{k}$			*		V/V	
Gain Equation			$G = 5 + 200\text{k}\Omega/R_G$			*		V/V	
Gain Error	$G = 5$		± 0.05	± 0.1		*	± 0.15	%	
vs Temperature	$G = 5$		5	10		*	*	$\text{ppm}/^\circ\text{C}$	
Gain Error	$G = 100$		± 0.3	± 0.5		*	± 1	%	
vs Temperature	$G = 100$		± 25	± 100		*	*	$\text{ppm}/^\circ\text{C}$	
Nonlinearity	$G = 100, V_O = -14.85\text{V to } +14.9\text{V}$		± 0.005	± 0.012		*	± 0.024	%	
NOISE (RTI)									
Voltage Noise, $f = 1\text{kHz}$			60			*		$\text{nV}/\sqrt{\text{Hz}}$	
$f = 100\text{Hz}$			100			*		$\text{nV}/\sqrt{\text{Hz}}$	
$f = 10\text{Hz}$			110			*		$\text{nV}/\sqrt{\text{Hz}}$	
$f_B = 0.1\text{Hz to } 10\text{Hz}$			2			*		$\mu\text{Vp-p}$	
Current Noise, $f = 1\text{kHz}$			80			*		$\text{fA}/\sqrt{\text{Hz}}$	
$f_B = 0.1\text{Hz to } 10\text{Hz}$			2			*		pAp-p	
OUTPUT									
Voltage, Positive	$V_O = \pm 15\text{V}$	$(V^+) - 0.1$	$(V^+) - 0.05$		*	*		V	
Negative	$V_O = \pm 15\text{V}$	$(V^-) + 0.15$	$(V^-) + 0.1$		*	*		V	
Short-Circuit Current	Short-Circuit to Ground		$+3/-30$			*		mA	
Capacitive Load Drive			1			*		nF	
FREQUENCY RESPONSE									
Bandwidth, -3dB	$G = 5$		120			*		kHz	
	$G = 100$		5			*		kHz	
	$G = 500$		0.9			*		kHz	
Slew Rate			$+0.08/-0.16$			*		$\text{V}/\mu\text{s}$	
Settling Time, 0.01%	$G = 5$		350			*		μs	
	$G = 100$		450			*		μs	
	$G = 500$		1.8			*		ms	
Overload Recovery	50% Input Overload		3			*		μs	
POWER SUPPLY									
Voltage Range, Single Supply		+2.2	+5	+36	*	*	*	V	
Dual Supplies		-0.9/+1.3		± 18	*	*	*	V	
Current	$I_O = 0$		60	85		*	*	μA	
TEMPERATURE RANGE									
Specification		-40		+85	*		*	$^\circ\text{C}$	
Operation		-55		+85	*		*	$^\circ\text{C}$	
Storage		-55		+125	*		*	$^\circ\text{C}$	
Thermal Resistance, θ_{JA}									
8-Pin DIP			150			*		$^\circ\text{C}/\text{W}$	
SO-8 Surface-Mount			150			*		$^\circ\text{C}/\text{W}$	

* Specification same as INA122P, INA122U.

Fig. A.2: INA122 data sheet

PIN CONFIGURATION



ELECTROSTATIC DISCHARGE SENSITIVITY

This integrated circuit can be damaged by ESD. Burr-Brown recommends that all integrated circuits be handled with appropriate precautions. Failure to observe proper handling and installation procedures can cause damage.

ESD damage can range from subtle performance degradation to complete device failure. Precision integrated circuits may be more susceptible to damage because very small parametric changes could cause the device not to meet its published specifications.

ABSOLUTE MAXIMUM RATINGS⁽¹⁾

Supply Voltage, V^+ to V^-	36V
Signal Input Terminals, Voltage ⁽²⁾	$(V^-)-0.3V$ to $(V^+)+0.3V$
Current ⁽²⁾	5mA
Output Short Circuit	Continuous
Operating Temperature	-40°C to $+125^\circ\text{C}$
Storage Temperature	-55°C to $+125^\circ\text{C}$
Lead Temperature (soldering, 10s)	$+300^\circ\text{C}$

NOTES: (1) Stresses above these ratings may cause permanent damage.
 (2) Input terminals are internally diode-clamped to the power supply rails. Input signals that can exceed the supply rails by more than 0.3V should be current-limited to 5mA or less.

PACKAGE INFORMATION

PRODUCT	PACKAGE	PACKAGE DRAWING NUMBER ⁽¹⁾
INA122PA	8-Pin DIP	006
INA122P	8-Pin DIP	006
INA122UA	SO-8 Surface Mount	182
INA122U	SO-8 Surface Mount	182

NOTE: (1) For detailed drawing and dimension table, see end of data sheet, or Appendix C of Burr-Brown IC Data Book.

Fig. A.3: INA122 data sheet

Platinum Resistance Temperature Detector

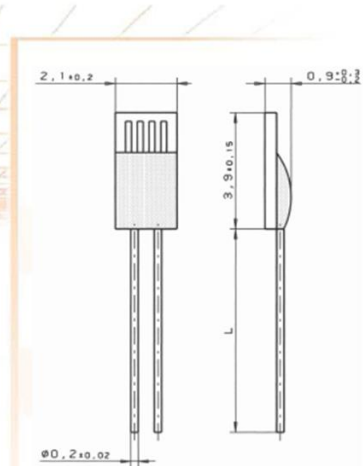
M 422

M series PRTDs are especially robust and are designed for large volume applications where long term stability, interchangeability and accuracy over a large temperature range are vital. Typical applications are Automotive, White Goods, HVAC, Energy Management, Medical and Industrial Equipment.

Nominal Resistance R_0	Tolerance	Order No. Plastic bag	Order No. Blister reel
100 Ohm at 0°C	DIN EN 60751, class B	32 208 392	32 208 520
	DIN EN 60751, class A	32 208 498	32 208 521
	DIN EN 60751, class 1/3 DIN	32 208 500	32 208 522
500 Ohm at 0°C	DIN EN 60751, class B	32 208 414	32 208 523
	DIN EN 60751, class A	32 208 501	32 208 524
	DIN EN 60751, class 1/3 DIN	32 208 502	32 208 525
1000 Ohm at 0°C	DIN EN 60751, class B	32 208 499	32 208 526
	DIN EN 60751, class A	32 208 503	32 208 527
	DIN EN 60751, class 1/3 DIN	32 208 537	

The measuring point for the nominal resistance is defined at 8 mm from the end of the sensor body.

Specification	DIN EN 60751 (according to IEC 751)	
Temperature range	-70°C to +500°C (continuous operation) (temporary use to 550 °C possible) Tolerance class B: - 70 °C to + 500 °C Tolerance class A: - 50 °C to + 300 °C Tolerance class 1/3 DIN: 0 °C to + 150 °C	
Temperature coefficient	TC = 3850 ppm/K ; 3750 ppm/K available on request	
Leads	Pt clad Ni wire Recommend connection technology: Welding, Crimping and Brazing	
Lead lengths (L)	10 mm +/- 1 mm	
Longterm stability	max. R_0 -drift 0.04% after 1000 h at 500 °C	
Vibration resistance	at least 40 g acceleration at 10 to 2000 Hz, depends on installation	
Shock resistance	at least 100 g acceleration with 8ms half sine wave, depends on installation	
Environmental conditions	unhoused for dry environments only	
Insulation resistance	> 100 MΩ at 20 °C; > 2 MΩ at 500 °C	
Self heating	0.3 K/mW at 0 °C	
Response time	water current (v = 0.4 m/s):	$t_{0.5} = 0.07$ s $t_{0.9} = 0.20$ s
	air stream (v = 2 m/s):	$t_{0.5} = 3.2$ s $t_{0.9} = 11$ s
Measuring current	100 Ω: 0.3 to 1.0 mA 500 Ω: 0.1 to 0.7 mA 1000 Ω: 0.1 to 0.3 mA (self heating has to be considered)	
Note	Other tolerances, values of resistance and wire lengths are available on request.	



We reserve the right to make alterations and technical data printed. All technical data serves as a guideline and does not guarantee particular properties to any products.

Heraeus Sensor Technology GmbH, Reinhard- Heraeus- Ring 23, 63801 Kleinostheim, Germany
Phone: +49 (0) 6181/35-8098, Fax: +49 (0)6181/35-8101, E-Mail: info.HSND@Heraeus.com Web: www.heraeus-sensor-technology.com

name of document: 30910021 Index A
Status: 09/2008

Fig. A.4: PT-1000 sensor data sheet



3M™ Thermally Conductive Adhesive Tape 8940 / 8943

Product Information Sheet

11.04.2007

Supersedes Version 01.10.2005

Product Description 3M™ Thermally Conductive Adhesive Tapes 8940 / 8943 are designed to provide an efficient heat transfer path between heat generating components and heat sinks or other cooling devices.

The tapes consist of a carrier, highly loaded with thermally conductive fillers, coated on either one side (3M™ 8943) or both sides (3M™ 8940) with a high temperature resistance acrylic pressure sensitive adhesive.

The specialized construction securely bonds the heat generating components to heat sinks and offer both, good thermal conductivity and excellent electrical insulation properties.

Product Construction

	3M 8940	3M 8943
Color	Beige	
Carrier	Filled Copolymer	
Adhesive type	Modified Acrylic Adhesive	
Tape type	Double coated	Single coated
Tape Thickness	0.190mm	0.170 mm
Liner Thickness	0,075 mm	

The film liner is a double sided siliconized Polyester Film with a differential release system.

20.996 x 29.700 厘米

Typical Applications Applications requiring good thermal transfer and thin bonding. Typical applications are assembling of power devices as bare dies in chip on board technique or flip chip assemblies with a directly mounted heat sink. The tape performance properties have been primarily adapted to fit thermal requirements in applications such as Engine Control Units bonding, ABS Systems, High power LED's, and other electronic increased power devices.

Fig. A.5: 3M tape data sheet

Typical Properties and Performance Characteristics

Note: The following technical information for 3M™ Thermally Conductive Tape 8940 / 8943 should be considered representative or typical only and should not be used for specification purposes.

Thermal Properties	Test	Unit	Value		Test Method
	Thermal Conductivity at 25 °C		W/m*K	0,9	
Coefficient of Thermal Expansion (-40 to 150°C)		mm/°C	140 E -06		TMA

Electrical Properties	Test	Unit	Value		Test Method
			8940	8943	
Breakdown Voltage typical value *		kV	10.3	9.8	IEC 60243-1
Dielectric Strength typical value *		kV/mm	55	52	IEC 60243-1
Volume Resistivity		Ω*cm	2,5 x 10 ¹³		ASTM D257

* Average value (not for specification purposes)

Mechanical Properties	Test	Unit	Value		Test Method
	90° Peel Adhesion to Aluminium Substrate (AlMgs; R _a : 0,48 μm; R _c :)μm)	20 min dwell time at room temp.	N/cm	5,0	
24 h dwell time room temp.		N/cm	6,0		AFERA 5001
at 150 °C		N/cm	4,9		AFERA 5001
at 180 °C		N/cm	2,4		AFERA 5001
Overlap Shear	20 min dwell time at room temp.	MPa	5,3		ASTMD 1002
	24 h dwell time room temp.	MPa	9,0		ASTMD 1002
	After 24 h @ 150 °C	MPa	6,8		ASTMD 1002
	After 24 h @ - 40 °C	MPa	9,0		ASTMD 1002
Holding Power	1000 g load @ room temp.	Minutes	10000+		AFERA 4012
	500 g load @ 70 °C	Minutes	10000+		AFERA 4012
Tensile strength	Tensile Strength	N/mm ²	6-7		EN ISO 527-2
	Elongation at break	%	80-120		EN ISO 527-2
Liner properties	Liner release	cN/25,4 mm	15		FINAT TM3
Temperature Performance	Thermal Stability 225 °C Dwell @ 60 min (Tape was applied between a glass and an aluminium panel)	Visual	No Change		3M
	Solder Reflow process according to JEDEC J-STD-020C (Level 1)	Visual	Test in process		3M
	Continuous Operating Temperature Range	°C	- 40 up to 150		3M

Fig. A.6: 3M tape data sheet

Appendix B

Matlab code

```

% *****
% Relationship between Vout and Rt
% for Fig. 3.2
% HUANG JUNXING
% *****
R=1000;
Vin=7.5;
Rt=0:10:7000
siz=size(Rt);
Ni=siz(2);
for i=1:Ni
    Vout(i)=(Rt(i)/(Rt(i)+R)-1/2)*Vin;
end
plot(Rt,Vout)
grid

% *****
% Bode diagram of the amplitude-frequency response and the phase-frequency response
% for Fig. 3.5
% HUANG JUNXING
% *****
num=[0,1];% numerator
den=[0.47,1];% denominator
system=tf(num,den);
bode(system)
grid

% *****
% Calibration Data Handling
% 20-04-2014
% HUANG JUNXING
% *****
clear
close all
clc
load temperature3.txt;
loadfile=temperature3;
% Load the data into each channel
Tem=loadfile(:,1);
ch0=loadfile(:,2);
ch1=loadfile(:,3);
ch2=loadfile(:,4);
ch3=loadfile(:,5);
ch4=loadfile(:,6);
ch5=loadfile(:,7);
ch6=loadfile(:,8);
ch7=loadfile(:,9);
% Draw the Polynome for each Channel
Fitch0=fit(ch0,Tem,'poly2')
Fitch1=fit(ch1,Tem,'poly2')
Fitch2=fit(ch2,Tem,'poly2')
Fitch3=fit(ch3,Tem,'poly2')
Fitch4=fit(ch4,Tem,'poly2')
Fitch5=fit(ch5,Tem,'poly2')
Fitch6=fit(ch6,Tem,'poly2')

```

```

Fitch7=fit(ch7,Tem,'poly2')
V=[0:0.1:3.5];
T0=Fitch0(V);
T1=Fitch1(V);
T2=Fitch2(V);
T3=Fitch3(V);
T4=Fitch4(V);
T5=Fitch5(V);
T6=Fitch6(V);
T7=Fitch7(V);
% Plot the theoretical curve
A=3.9080*10^(-3);
B=-5.8019*10^(-7);
C=-4.2735*10^(-12);
R=1000;
R0=1000;
Vout2=[0:0.1:3.5];
Vout1=Vout2/5; %The time of the amplifier INA122 equal 5
Vin=4.93; %The output voltage of the 78L05 is 4.93
Ni=length(Vout1)
for i=1:Ni
    Rt(i)=((2*Vout1(i)+Vin)*R)/(Vin-2*Vout1(i));
    Ttheory(i)=(-R0*A+sqrt((R0*A)^2-4*R0*B*(R0-Rt(i))))/(2*R0*B);
end

%Plot Channel 0
subplot(4,2,1)
plot(V,T0,'k','linewidth',1.5)
title('T0= 5.578V^2 + 38.83V + 0.4425')
hold on
plot(Vout2,Ttheory,'r','linewidth',2)
plot(ch0,Tem,'*')
grid on
legend('Fitting curve','Theoretical curve','Calibration value')

%Plot Channel 1
subplot(4,2,2)
plot(V,T1,'k','linewidth',1.5)
title('T1= 5.567V^2 + 38.86V + 0.3545')
hold on
plot(Vout2,Ttheory,'r','linewidth',2)
plot(ch1,Tem,'*')
grid on

%Plot Channel 2
subplot(4,2,3)
plot(V,T2,'k','linewidth',1.5)
title('T2= 5.573V^2 + 38.88V + 0.3973')
hold on
plot(Vout2,Ttheory,'r','linewidth',2)
plot(ch2,Tem,'*')
grid on

%Plot Channel 3
subplot(4,2,4)

```

```

plot(V,T3,'k','linewidth',1.5)
title('T3= 5.548V^2 + 38.93V + 0.4366')
hold on
plot(Vout2,Ttheory,'r','linewidth',2)
plot(ch3,Tem,'*')
grid on

%Plot Channel 4
subplot(4,2,5)
plot(V,T4,'k','linewidth',1.5)
title('T4= 5.569V^2 + 38.83V + 0.4987')
hold on
plot(Vout2,Ttheory,'r','linewidth',2)
plot(ch4,Tem,'*')
grid on

%Plot Channel 5
subplot(4,2,6)
plot(V,T5,'k','linewidth',1.5)
title('T5= 5.585V^2 + 38.75V + 0.4796')
hold on
plot(Vout2,Ttheory,'r','linewidth',2)
plot(ch5,Tem,'*')
grid on

%Plot Channel 6
subplot(4,2,7)
plot(V,T6,'k','linewidth',1.5)
title('T6= 5.509V^2 +39.08V + 0.4723')
hold on
plot(Vout2,Ttheory,'r','linewidth',2)
plot(ch6,Tem,'*')
grid on

%Plot Channel 7
subplot(4,2,8)
plot(V,T7,'k','linewidth',1.5)
title('T7= 5.527V^2 + 38.89V + 0.2754')
hold on
plot(Vout2,Ttheory,'r','linewidth',2)
plot(ch7,Tem,'*')
grid on

%*****
% T=f(t),5.2.1
% for Fig. 5.7-Fig. 5.9
% HUANG JUNXING
%*****
clear
close all
clc

%No1
load coreheating1326.txt;
loadfile=coreheating1326;

```

```

N=33440;

%No2
% load coreheating1426.txt;
% loadfile=coreheating1426;
% N=25192;

%No3
% load coreheating1526.txt;
% loadfile=coreheating1526;
% N=26648;

for i=1:(N-1)/8
    T1(i)=loadfile(8*i+1,2);
    T2(i)=loadfile(8*i+2,2);
    T3(i)=loadfile(8*i+3,2);
    T4(i)=loadfile(8*i+4,2);
    T5(i)=loadfile(8*i+5,2);
    TY(i)=loadfile(8*i+6,2);
    TC(i)=loadfile(8*i+7,2);
    TA(i)=loadfile(8*i+8,2);
end

k=length(T1);
x=1:k
plot(x,TC,x,T1,x,T2,x,T3,x,T4,x,T5,x,TY,x,TA,'red','linewidth',1)
xlabel('time[s]')
ylabel('temperature[ ºe]')
legend('TC','T1','T2','T3','T4','T5','TY','TA')
axis([0 4000 0 85])
grid

% *****
% Rth=f(t),5.2.1
% for Fig. 5.10-Fig. 5.12
% HUANG JUNXING
% *****

clear
close all
clc
%No1
load coreheating1326.txt;
loadfile=coreheating1326;
N=33440;
P=3.86508;

%No2
% load coreheating1426.txt;
% loadfile=coreheating1426;
% N=25192;
% P=2.40345;

%No3
% load coreheating1526.txt;

```

```

% loadfile=coreheating1526;
% N=26648;
% P=1.68018;

for i=1:(N-1)/8
    T1(i)=loadfile(8*i+1,2);
    T2(i)=loadfile(8*i+2,2);
    T3(i)=loadfile(8*i+3,2);
    T4(i)=loadfile(8*i+4,2);
    T5(i)=loadfile(8*i+5,2);
    TY(i)=loadfile(8*i+6,2);
    TC(i)=loadfile(8*i+7,2);
    TA(i)=loadfile(8*i+8,2);
end

RthC1=(TC-T1)/P;
Rth12=(T1-T2)/P;
Rth23=(T2-T3)/P;
Rth34=(T3-T4)/P;
Rth45=(T4-T5)/P;
Rth5Y=(T5-TY)/P;
RthYA=(TY-TA)/P;

k=length(T1);
x=1:k
plot(x,RthC1,x,Rth12,x,Rth23,x,Rth34,x,Rth45,x,Rth5Y,x,RthYA,'linewidth',3)
legend('RthC1','Rth12','Rth23','Rth34','Rth45','Rth5Y','RthYA')
xlabel('time[s]')
ylabel('thermal resistance[k/w]')
axis([0 4000 0 3.5])
grid

% *****
% Mesh-Current-Analysis for the heat network,5.2.2
% for Table 5.6
% HUANG JUNXING
% *****

clc
close all
clear all

Rtotal=25.0808431450213;
RC1=14.9896738074409;
R12=1.29654886395014;
R23=0.139566655661111;
R34=0.0261246739263876;
R45=0.445597388536415;
R5Y=1.1525258110241;
RYA=7.03080594448218;

% test1
TA=30.6651902;
P1=0.492406530612245;
P2=0.534808204081633;
P3=0.547118367346939;

```

```
P4=0.588152244897959;
P5=0.652438653061225;
```

```
% % test2
% TA=31.9106088;
% P1=1.39645014577259;
% P2=1.51670001943635;
% P3=1.55161127308066;
% P4=1.66798211856171;
% P5=1.85029644314869;
```

```
% % test3% TA=33.0970498;
% P1=2.11004081632653;
% P2=2.2917387755102;
% P3=2.34448979591837;
% P4=2.52032653061224;
% P5=2.79580408163265;
```

```
PL1=P1;
PL2=PL1+P2;
PL3=PL2+P3;
PL4=PL3+P4;
PL5=PL4+P5;
```

```
T1=T2+R12*PL1;
T2=T3+R23*PL2;
T3=T4+R34*PL3;
T4=T5+R45*PL4;
T5=(R5Y+RYA)*PL5;
TY=RYA*PL5;
```

```
[T1,T2,T3,T4,T5,TY]=solve('T1=T2+R12*PL1','T2=T3+R23*PL2','T3=T4+R34*PL3','T4=T5+R45*
PL4','T5=(R5Y+RYA)*PL5','TY=RYA*PL5')
```

```
% *****
% Difference between theoretical and measured values,5.2.2
% for Fig. 5.15-Fig. 5.17
% HUANG JUNXING
% *****
```

```
clear
close all
clc
%No.1
load wingdingheating1634.txt;
loadfile=wingdingheating1634;
N=25584;
P=2.814924;
T1_theory=55.49;
T2_theory=54.71;
T3_theory=54.71;
T4_theory=54.66;
T5_theory=53.70;
TY_theory=50.46;
TA=30.67;
```

```

%No.2
% load wingdingheating1735.txt;
% loadfile=wingdingheating1735;
% N=26880;
% P=7.98304;
% T1_theory= 102.31 ;
% T2_theory= 100.49 ;
% T3_theory= 100.09 ;
% T4_theory= 99.97 ;
% T5_theory= 97.24 ;
% TY_theory= 88.04 ;
% TA= 31.91 ;

%No.3
% load wingdingheating1836.txt;
% loadfile=wingdingheating1836;
% N=26784;
% P=12.0624;
% T1_theory= 139.46 ;
% T2_theory= 136.73 ;
% T3_theory= 136.11 ;
% T4_theory= 135.94 ;
% T5_theory= 131.81 ;
% TY_theory= 117.91 ;
% TA= 33.10 ;

for i=1:(N-1)/8
    T1(i)=loadfile(8*i+1,2);
    T2(i)=loadfile(8*i+2,2);
    T3(i)=loadfile(8*i+3,2);
    T4(i)=loadfile(8*i+4,2);
    T5(i)=loadfile(8*i+5,2);
    TY(i)=loadfile(8*i+6,2);
    TC(i)=loadfile(8*i+7,2);
    TA(i)=loadfile(8*i+8,2);
end

k=length(T1);
x=1:k;
subplot(3,2,1)
plot(x,T1,'blue',x,T1_theory,'red','linewidth',2)
legend('T1 measurement','T1 theory')
xlabel('time[s]')
ylabel('temperature[ ºe]')
axis([0 3200 0 65]),grid

subplot(3,2,2)
plot(x,T2,'blue',x,T2_theory,'red','linewidth',2)
legend('T2 measurement','T2 theory')
xlabel('time[s]')
ylabel('temperature[ ºe]')
axis([0 3200 0 65]),grid

subplot(3,2,3)
plot(x,T3,'blue',x,T3_theory,'red','linewidth',2)

```

```

legend('T3 measurement','T3 theory')
xlabel('time[s]')
ylabel('temperature [ ºe]')
axis([0 3200 0 65]),grid

subplot(3,2,4)
plot(x,T4,'blue',x,T4_theory,'red','linewidth',2)
legend('T4 measurement','T4 theory')
xlabel('time[s]')
ylabel('temperature [ ºe]')
axis([0 3200 0 65]),grid

subplot(3,2,5)
plot(x,T5,'blue',x,T5_theory,'red','linewidth',2)
legend('T5 measurement','T5 theory')
xlabel('time[s]')
ylabel('temperature [ ºe]')
axis([0 3200 0 65]),grid

subplot(3,2,6)
plot(x,TY,'blue',x,TY_theory,'red','linewidth',2)
legend('TY measurement','TY theory')
xlabel('time[s]')
ylabel('temperature [ ºe]')
axis([0 3200 0 65]),grid

% *****
% Coil former test,5.3.2
% for Fig. 5.27-Fig. 5.29
% HUANG JUNXING
% *****
clear
close all
clc
% NO1
load coilformer1001.txt;
loadfile=coilformer1001;
N=31840;
P=1.597*1.352;

%NO2
% load coilformer1101.txt;
% loadfile=coilformer1101;
% N=27744;
% P=1.816*1.596;
%NO3
% load coilformer1208.txt;
% loadfile=coilformer1208;
% N=31176;
% P=2.016*1.748;

for i=1:(N-1)/8
    T1(i)=loadfile(8*i+1,1);
    T2(i)=loadfile(8*i+2,1);
    T3(i)=loadfile(8*i+3,1);

```

```

T4(i)=loadfile(8*i+4,1);
T5(i)=loadfile(8*i+5,1);
TY(i)=loadfile(8*i+6,1);
TC(i)=loadfile(8*i+7,1);
TA(i)=loadfile(8*i+8,1);
end
Rthc1=(T1-TC)/1000000/P;
Rth_theory=2.724867;
k=length(T1);
x=1:k
plot(x,Rthc1,'linewidth',3)
hold on
plot(x,Rth_theory,'red','linewidth',3)
legend('Measured Rthc1','Theoretical Rthc1')
xlabel('time[s]')
ylabel('thermal resistance[k/w]')
axis([0 4000 0 3.5])
grid
gtext('Rth theory=2.725')

% *****
% Core test,5.3.3
% for Fig. 5.35-Fig. 5.37
% HUANG JUNXING
% *****
clear
close all
clc
% %NO1
load core1652.txt;
loadfile=core1652;
N=28424;
P=1.595*1.264;

%NO2
% load core1749.txt;
% loadfile=core1749;
% N=26752;
% P=1.813*1.396;
%NO3
% load core1844.txt;
% loadfile=core1844;
% N=24088;
% P=2.018*1.508;

for i=1:(N-1)/8
    T1(i)=loadfile(8*i+1,1);
    % T2(i)=loadfile(8*i+2,1);
    % T3(i)=loadfile(8*i+3,1);
    % T4(i)=loadfile(8*i+4,1);
    % T5(i)=loadfile(8*i+5,1);
    % TY(i)=loadfile(8*i+6,1);
    TC(i)=loadfile(8*i+7,1);
    % TA(i)=loadfile(8*i+8,1);
end

```

```

Rthc1=(T1-TC)/P;
Rth_theory=4.0251;
k=length(T1);
x=1:k
plot(x,Rthc1,'linewidth',3)
% axis([0 3500 2.5 3.5])
hold on
plot(x,Rth_theory,'red','linewidth',3)
legend('Measured Rth core','Theoretical Rth core')
xlabel('time[s]')
ylabel('thermal resistance[k/w]')
axis([0 4000 0 4.5])
grid
gtext('Rth theory=4.0251')

% *****
% Winding test,5.3.4
% for Fig. 5.39-Fig. 5.41
% HUANG JUNXING
% *****

clear
close all
clc
% %NO1
load allwinding1250.txt;
loadfile=allwinding1250;
N=39824;
P=1.4055;

%NO2
% load allwinding1409.txt;
% loadfile=allwinding1409;
% N=36920;
% P=1.9511;
%NO3
% load allwinding1515.txt;
% loadfile=allwinding1515;
% N=30432;
% P=2.9625;
for i=1:(N-1)/8
    T1(i)=loadfile(8*i+1,1);
    TA(i)=loadfile(8*i+2,1);
    T2(i)=loadfile(8*i+3,1);
    T3(i)=loadfile(8*i+4,1);
    T4(i)=loadfile(8*i+5,1);
    T5(i)=loadfile(8*i+6,1);
    TC(i)=loadfile(8*i+7,1);
    TY(i)=loadfile(8*i+8,1);
end
Rth12=(T2-T1)/P;
Rth23=(T3-T2)/P;
Rth34=(T4-T3)/P;
Rth45=(T5-T4)/P;
Rth5Y=(TY-T5)/P;

```

```

Rth12_theory=0.9445;
Rth23_theory=0.8850;
Rth34_theory=0.8325;
Rth45_theory=0.6566;
Rth5Y_theory=0.6247;

k=length(T1);
x=1:k
subplot(3,2,1)
plot(x,Rth12,x,Rth12_theory,'red','linewidth',2)
legend('Rth12 measured','Rth12 theoretical'),grid
xlabel('time[s]')
ylabel('thermal resistance[k/w]')
axis([0 4000 0 1.2])

subplot(3,2,2)
plot(x,Rth23,x,Rth23_theory,'red','linewidth',2)
legend('Rth23 measured','Rth23 theoretical'),grid
xlabel('time[s]')
ylabel('thermal resistance[k/w]')
axis([0 4000 0 1.2])

subplot(3,2,3)
plot(x,Rth34,x,Rth34_theory,'red','linewidth',2)
legend('Rth34 measured','Rth34 theoretical'),grid
xlabel('time[s]')
ylabel('thermal resistance[k/w]')
axis([0 4000 0 1.2])

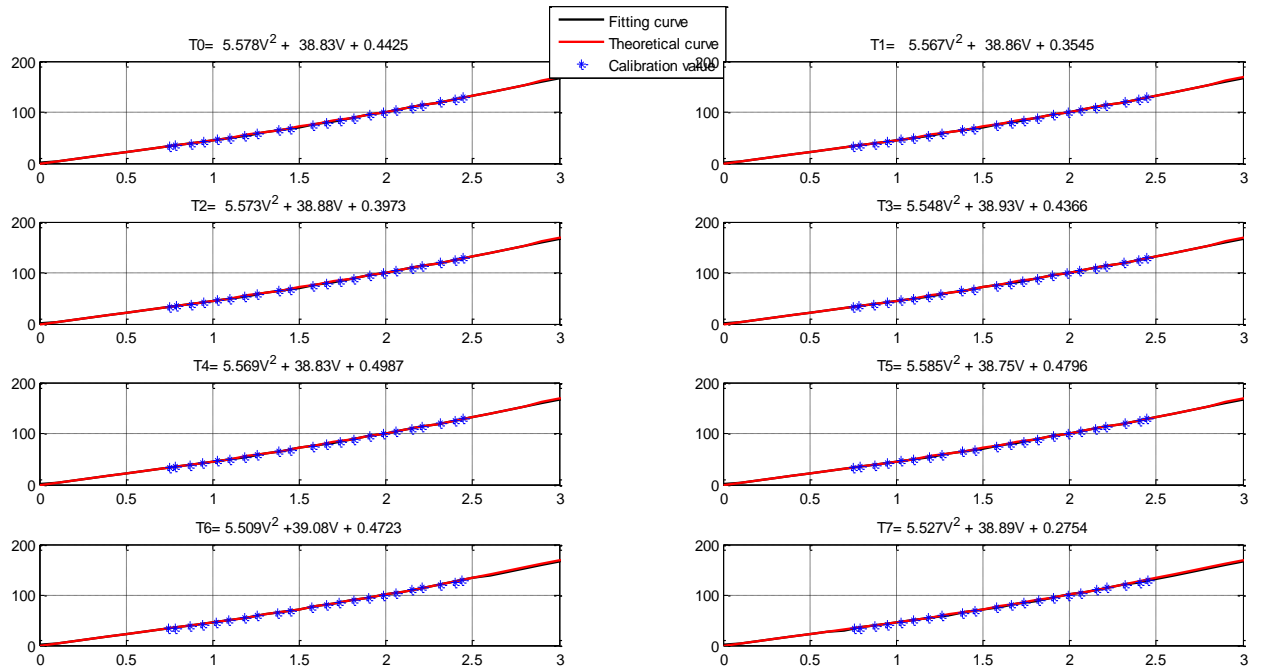
subplot(3,2,4)
plot(x,Rth45,x,Rth45_theory,'red','linewidth',2)
legend('Rth45 measured','Rth45 theoretical'),grid
xlabel('time[s]')
ylabel('thermal resistance[k/w]')
axis([0 4000 0 1.2])

subplot(3,2,5)
plot(x,Rth5Y,x,Rth5Y_theory,'red','linewidth',2)
legend('Rth5Y measured','Rth5Y theoretical'),grid
xlabel('time[s]')
ylabel('thermal resistance[k /w]')
axis([0 4000 0 1.2])

```

Appendix C

Quadratic function for each channel



Titre: Modèle thermique d'un transformateur à la base de capteur PT-1000

Title: Thermal Modelling of a Transformer based on PT-1000 Sensor

Université/University: Chalmers University of Technology

RESUME

Ce travail vise à la modélisation thermique d'un transformateur à enroulement multicouche à base de capteur de température PT-1000. Afin de réaliser cet objectif, d'une part, une brève introduction sur le système d'acquisition de données, y compris PCB et LabVIEW a été faite. Ensuite, deux tests ont été effectués principales. Pour la première, un transformateur sans aucune couche intermédiaire d'isolation thermique a été construit. Cet essai a porté sur la mesure de la résistance thermique à l'aide d'une source de chauffage externe afin de créer un flux de chaleur d'une seule dimension. Sur la base des résultats précédents, la température de chaque couche peut être prédite lorsque les enroulements ont été réalisés avec une puissance à courant continu dans l'application réelle. Ce modèle de prédiction appliqué à n'importe quelle DC courant, mais était uniquement pour le certain transformateur. Pour le deuxième essai, les résistances thermiques théoriques ont été calculées sur la base d'une part le matériau qui a été utilisé pour la fabrication du transformateur. Ensuite, la comparaison entre les valeurs théoriques et mesurées est accomplie. Le plus grand sens de ce modèle a menti sur l'applicabilité de tous les transformateurs similaires.

Lorsque toutes les résistances thermiques de chaque partie ont été décidées, le réseau thermique entier a été représenté

ABSTRACT

This work aims at the thermal modelling of a multilayer wire-wound transformer and its verification by using the temperature sensors of the type PT-1000. In order to achieve this goal, firstly, a brief introduction about the data acquisition system including PCB and LabVIEW was made. Then two main tests were carried out. For the first one, a transformer without any interlayer thermal insulation was constructed. This test focused on the measurement of thermal resistance by using an external heating source to create a one-dimension heat flow. On the basis of these results, the temperature of each layer could be predicted when the windings were conducted with DC power in the realistic application. This prediction model applied to any DC current but was only suitable for the transformer made in test 1. For the second test, the theoretical thermal resistances were firstly calculated based on the material which was used to manufacture the transformer. Then the comparison between the theoretical and measured values was performed. The most important usage of this model lied on the applicability to all the similar transformers.

When all the thermal resistances in each part were decided, a whole thermal network was presented.

Mots clés:

1. Modèle thermique
2. PT-1000
3. Transformateur
4. PLECS
5. LabVIEW

Key words:

1. Thermal Modelling
2. PT-1000
3. Transformer
4. PLECS
5. LabVIEW